African Corrosion Journal
Official publication of the Corrosion Institute of Southern Africa
www.africorr.org.za

Micro-galvanic corrosion of Ti-6Al-4V in situ alloyed with molybdenum via selective laser melting

C. Madikizela
Council for Scientific and Industrial Research,
National Laser Centre, Pretoria;
and University of the Witwatersrand, and DST-NRF Centre of Excellence in Strong Materials,
Johannesburg,
South Africa

L.H. Chown
University of the Witwatersrand, and DST-NRF Centre of Excellence in Strong Materials
1, Jan Smuts Avenue
Johannesburg,
South Africa

L.A. Cornish
University of the Witwatersrand, and DST-NRF Centre of Excellence in Strong Materials
1, Jan Smuts Avenue
Johannesburg,
South Africa

H. Moller
Council for Scientific and Industrial Research,
National Laser Centre, Pretoria;
Now at:
Department of Materials Science and Metallurgical Engineering, University of Pretoria,
Pretoria, 0001,
South Africa

ARTICLE INFO

Keywords:
Additive manufacturing
Selective laser melting
Ti-6Al-4V
Molybdenum

ABSTRACT

Powder-bed laser metal additive manufacturing via in situ alloying is currently of interest for alloy development. Molybdenum is a beta-stabilizer which is added to Ti-6Al-4V to produce a more ductile beta alloy. Previous studies have shown that in situ alloying of Ti-6Al-4V with Mo produced a composite consisting of a beta-stabilized matrix with some un-melted Mo particles. Although this microstructure did give better mechanical properties than without Mo, there was a concern that the composite could experience possible micro-galvanic corrosion effects, since Ti-6Al-4V is more noble on the galvanic series than Mo. Immersion tests were done on a composite sample placed in a 3.5% NaCl solution, and a scanning electron microscope was used to examine the corrosion effects weekly. Corrosion attack of the anodic Mo particles was found, whereas there was little effect on the matrix. The resulting composite microstructure might therefore be beneficial for improving mechanical properties, but its corrosion resistance might be problematic in certain applications.

1. Introduction

Additive manufacturing has rapidly developed since the invention of lasers in the 1960s. This technology has benefited from extensive research, especially for applications in the manufacturing industry where the benefits of lower material wastage, higher production efficiencies and infinite possible geometries can maximize profit [1]. For this reason, selective laser melting (SLM) processes have gained preference over conventional methods (e.g. casting) in the manufacturing industry. These processes involve the use of a CAD model to design and "slice" the part into layers. A laser is then used to melt the

powder deposited, and raked according to the thickness of each layer, according to the design [1, 2].

In recent studies [3, 4, 5], selective laser melting has been used to investigate its capabilities in directly developing new complex materials to improve mechanical properties. Factors which are essential in the improvement of mechanical properties include strengthening through reinforcement, incitement of nucleation, refinement of the microstructure to produce manufactured parts with no porosity or defects [6]. Vrancken et al. [4] added 10 wt% Mo to Ti-6Al-4V to stabilize the beta phase and therefore increase the ductility and fracture toughness of the alloy. Processing at higher speeds and power compared to Vrancken et al. [4], Madikizela et al. [7] manufactured the same alloy. The microstructure of alloys produced in situ via the SLM process often had some inhomogeneities, especially un-melted Mo particles in the as-built state [3, 4, 5, 7].

The resultant (composite-like) as-built microstructure gave rise to questions around the corrosion resistance of such a microstructure. This topic has not been reported by other researchers in the field [4, 5].

Galvanic corrosion results from the contact between two different conducting materials in a corrosive environment [8]. This type of corrosion is commonly found in ships where the parts immersed in the sea water are made of various metal alloys or metal matrix composite materials, where the reinforcing material is spread throughout the metal, e.g. graphite [8]. Galvanic corrosion may result in the accelerated deterioration of one metal or the corrosion protection of a connected metal (anodic protection) [8]. Galvanic corrosion is not only affected by the potential difference between the two metals in contact, and other metallurgical factors such as surface conditions, electrolyte properties, reactions, environmental effects and geometric factors also play a part [8].

Considering Ti-6Al-4V and molybdenum, a galvanic series prepared by the U.S. Army Missile Command [9] revealed a significant difference in position between Ti-6Al-4V and Mo, which is a cause for concern. On this specific series [9], Ti-6Al-4V was number 85 while Mo was number 58, therefore the contact between these two dissimilar metals would be conducive for galvanic corrosion in the right environment, thus potentially resulting in the corrosion of the anodic Mo.

This work investigated the micro-galvanic effects between Ti-6Al-4V and Mo in a 3.5% NaCl solution for a sample in situ alloyed by the selective laser melting process.

2. Experimental Procedure

2.1. Powder mixing and SLM sample manufacturing

A 200g powder mixture was prepared by mixing 190g of Ti-6Al-4V powder (20-60µm) and 10g molybdenum powder (20-45µm) in a tubular mixer for 30 minutes [7]. An SLM machine containing a 5kW Nd Yag fiber laser with a 250µm spot size was used to produce 10x10mm samples under a protective argon atmosphere [7]. The samples were manufactured at a laser power of 1.3kW, at a laser scan speed of 4m/s, with a layer thickness of 50µm and a hatch overlap of 50% [7].

2.2. Micro-galvanic tests

108.8g of sodium chloride was dissolved in 3000ml of distilled water to make a 3.5% NaCl solution in a 5 litre plastic bucket. The area of study was identified by drawing a circle on the sample using the diamond indenter of a Vicker's hardness machine prior to immersion. This meant that the same area could be studied after each immersion. The sample was tied with non-conductive thread and the other end of the thread was tied to a rod which was placed across the top of the bucket. The polished sample was then submerged in the prepared 3.5% NaCl solution. The experiment was evaluated weekly for 20 weeks, accompanied by stirring the solution twice a day in order to make sure there was sufficient oxygen for the reaction, and the solution was replenished weekly to compensate for evaporation. After removing the sample, an SEM was used to examine the weekly changes, and then the sample was replaced in the bucket. Initially, the sample was weighed, but this was discontinued, because no difference was found,

since the proportion of the Mo particles was too small for the effect to be clearly observed.

2.3. Microstructural characterization

To better reveal the grain structure of un-melted Mo particle, the sample was etched with a solution of 10ml glycerol, 10ml HNO3 and 10ml HF for 5 minutes. The sample was investigated using an Olympus BX51M optical microscope (OM) and a JEOL JSM-6010PLUS/LA Scanning electron microscope (SEM).

3.0 Results and Discussions

3.1 Powder mixing

Mixing of Ti-6Al-4V and molybdenum powders gave a near-homogenous mixture as shown in Figure 1. The morphology of both Ti-6Al-4V and Mo powders was spherical. This is an ideal morphology, since particles with a spherical morphology are associated with forming good bonding between individual laser tracks, which leads to denser parts and increased component quality [6]. Segregation was found at a smaller scale, e.g. 200x magnification which is expected as 100% homogeneity cannot be obtained by mixing.

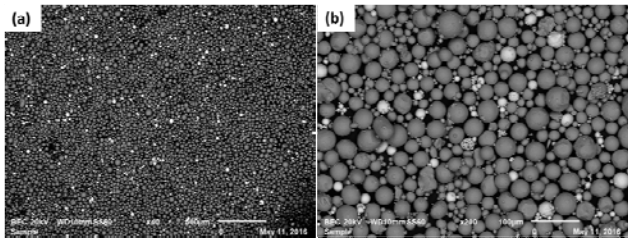

Figure 1: SEM-BEC images showing particle shape and morphology of Ti-6Al-4V+10M: (a) at lower magnification, and (b) at higher magnification, where the Mo particles have lighter contrast.

3.2 Microstructural analysis

Although adding 10 wt% Mo was supposed to fully stabilize the beta phase [4], Madikizela et al. [4] found from XRD that alpha peaks were still present for the microstructure (Figure 2). This was attributed to the poor melting of Mo at the manufacturing parameters, which gave Mo peaks in the XRD pattern, as well as some alpha peaks (Figure 2). This indicated that higher laser power and especially the higher scanning speeds than Vrancken et al. [4], were not sufficient to properly melt the Mo powder. The microstructure also showed pronounced melt pool boundaries showing the separate tracks as the sample was built, and darker contrast areas in backscattered electron mode with lower Mo contents, and light contrast areas where Mo was dissolved (Figure 2) [7]. Also, although the starting Mo powder particles were spherical initially (Figure 1), some had circular cross-sections in Figure 2(b), whereas some did not, indicating that some reaction had occurred, but not homogeneously throughout the sample. Xu et al. [10] discussed the XRD pattern of as-built Ti-6Al-4V produced via SLM. The ά peaks were found at 36°, 38°, 40°, 53°, 57° and 64° 2θ angles [10]. The peaks in this work were found at 35°, 37°, 38°, 40°, 49°, 63°, 73° and 74° 2θ angles. Although some ά peaks correspond to the Ti-6Al-4V peaks found by Xu et al. [10], some have shifted and ά was found at new peaks for Ti-6Al-4V +10 wt% Mo. The shift in peaks is attributed to the partial dissolution of Mo into the matrix.

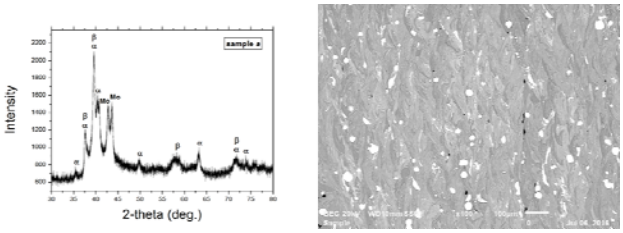

Figure 2: X-ray diffraction pattern and SEM-BEC image showing the microstructure of the sample [7].

Figure 3 (a) shows a section through an entire Mo powder particle in the matrix of the composite, and the circular cross-section was again similar to the shape of the starting powder in Figure 1. There was also a large hole in the centre (Figure 3 (a), and even in the un-etched condition, some of the grain boundaries could be resolved. Not all of the surface was smooth as in Figure 1 (albeit Figure 1 was at a much lower magnification), which suggested that possibly some melting of the Mo particle had occurred after all, but not enough to dissolve the entire particle in the matrix. Figure 3 (b) is a higher magnification image of the same Mo particle in the alloy, and reveals grains of different sizes and some porosity within the un-melted Mo-particle. There were also visible sub-grains inside the larger grains. The porosity in the Mo particle mainly occurred at the grain boundaries, and where it occurred within a grain, it was associated with the sub-grain boundaries. A similar grain structure was found for commercially pure Mo [11].

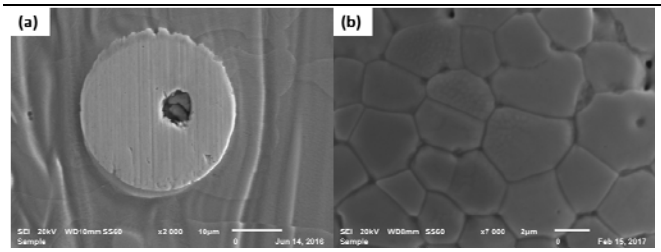

Figure 3: SEM-SE images showing an un-melted Mo particle: (a) whole un-etched Mo particle, and (b) etched Mo particle with grains and sub-grains within the particle.

3.3 Micro-galvanic corrosion

Figure 4 shows the progression of corrosion from week 1 to week 20. Comparing Figure 3(a) and Figure 4 (a), significant changes were evident as the particle had visible grain boundaries after a week, due to the corrosion attack. There was also an area of darker appearance in Figure 4 (a) where the corrosion was more severe than in other areas. After 20 weeks (Figure 4(b)), the particle was beginning to detach from the matrix and the prior grain boundaries were more pronounced and deeper. There was also evidence of sub-grain boundary attack (Figure 4(b)).

The grain size of the etched particle (Figure 3(b)) and the corroded particle Figure 4(a) was measured using the line intercept method. The average grain size for the etched sample was 2.9µm; this was lower than the average grain size found for the corroded particle from week 1 (3.6µm) (Figure 4(a)). This could be because the etchant works faster than the NaCl solution, hence more grains were revealed in the etched sample, or that the etchant just revealed the real microstructure better.

The difference in areas of the anodic and cathodic metals must also be considered. In this case, the total surface area of the corroding Mo metal was small compared to the area of the electropositive Ti-6Al-4V matrix. The corrosion reaction therefore occurred rapidly because of the increased oxygen reduction, which led to a greater galvanic current [12]. The smaller particles (1, 2 and 3) form Figure 4 (c and d) had corroded to the extent that they had fully detached from the matrix. The degradation of the larger particles (4 and 5 in Figure 4(c) and (d)) occurred due to detachment of grains/sub-grains within the Mo particles. This was followed by corrosion attack on the newly-exposed grain boundaries. This process repeated until the whole particle was detached from the matrix. Although the Mo particles corroded, the difference in the mass loss of the sample was too small to discern.

Dai et al. [13] studied the corrosion behaviour of a selective laser melted Ti-6Al-4V alloy in NaCl solution. In their work, the SLM-produced Ti-6Al-4V alloy showed inferior corrosion resistance than traditionally manufactured commercial Grade 5 Ti-6Al-4V [13]. This was attributed to the presence of the large fraction of acicular α phase compared to the β-Ti phase [13]. In the current study, the presence of Mo and its ability to stabilize the β phase was supposed to improve the corrosion properties of Ti-6Al-4V, but with the inhomogeneity in the microstructure, it introduced new problems. Therefore, further corrosion work needs to be done on the Ti-6Al-4V+10 wt% Mo alloy e.g. electrochemical measurements and polarization tests.

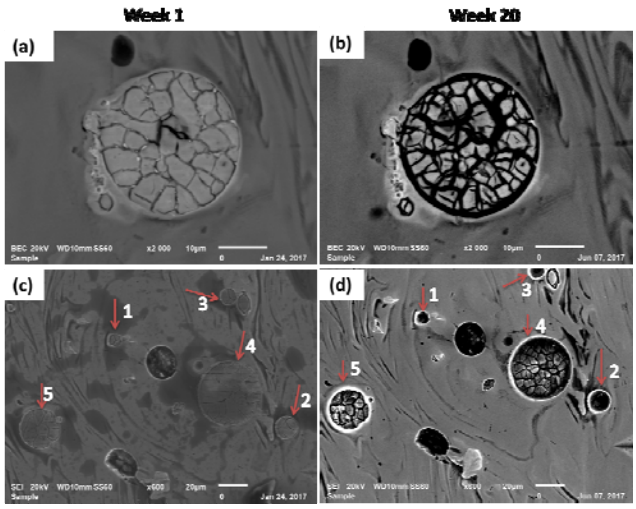

Figure 4: SEM-BEC and SEM-SE images showing the progression of corrosion: (a) and (c) high and low magnification images after immersion for 1 week, and (b) and (d) high and low magnification images after immersion for 20 weeks.

4. Conclusions

Although beneficial for the improvement of some mechanical properties in the as-built state, Ti-6Al-4V+10Mo in situ alloyed by SLM was susceptible to micro-galvanic corrosion in a 3.5% NaCl solution. This might limit the applications of this material in certain corrosive environments, and should be taken into consideration during material selection for specific applications.

Acknowledgements
The authors would like to thank the Department of Science and Technology, and the National Research Foundation, South Africa.

References

1. J. Kruth, M. Leu, T. Nakagawa, "Progress in Additive Manufacturing and Rapid Prototyping", CIRP Annals-Manufacturing Technology, 47(2) (1998): 525-540.

2. S. Kumar, S. Pityana, "Laser-Based Additive Manufacturing of Metals", http://researchspace.csir.co.za/dspace/bitstream/10204/4758/1/kumar6_2010.pdf (Sep. 14, 2016)

3. E. Chlebus, B. Kuznicka, R. Dziedzic, T. Kurzynowski, "Titanium alloyed with rhenium by selective laser melting", Materials Science & Engineering A, 620, (2015): 155-163.

4. B. Vrancken, L. Thijs, J. Kruth, J. Van Humbeeck, "Microstructure and Mechanical Properties of a Novel β Titanium Metallic Composite by Selective Laser Melting", Acta Materialia, 68 (2014): 150-158.

5. M. Fischer, D. Joguet, G. Robin, L. Peltier, P. Laheurte, "In situ Elaboration of a Binary Ti–26Nb Alloy by Selective Laser Melting of Elemental Titanium and Niobium Mixed Powders", Materials Science and Engineering: C, 62 (2016): 852-859.

6. H, Attar, M. Bönisch, M. Calin, L. Zhang, S. Scudino, J. Eckert, "Selective laser melting of in situ titanium–titanium boride composites: Processing, microstructure and mechanical properties", Acta Materialia, 76 (2014): 13-22.

7. C. Madikizela, L.A. Cornish, L.H. Chown, H. Moller, D. Louw, "Microstructure of in situ Alloyed Ti-6Al-4V and 10Mo as a Function of Process Parameters", Frontiers in Optics / Laser Science, Rochester NY, 2016.

8. X.G. Zhang, Galvanic Corrosion, in: R.W. Revie (Ed.) Uhlig's Corrosion Handbook, 3rd ed. (John Wiley & Sons, Inc.: Canada, 2011).

9. M.C. Farman and E.A. Verchot, "Practical galvanic series," U.S. Army missile command, Alabama, 1967.

10. W. Xu, M. Brandt, S. Sun, J. Elambasseril, Q. Liu, K. Latham, K. Xia, M. Qian, "Additive manufacturing of strong and ductile Ti–6Al–4V by selective laser melting via in situ martensite decomposition", Acta Materialia, 85 (2015): 74-84.

11. Y. Hiraoka, T. Hoshika, "Parameter representing low-temperature fracture strength in molybdenum having an elongated and large grain structure", (1999), http://www.sciencedirect.com/science/article/pii/S0263436899000189 (Sep. 14, 2016).

12. P.H. Hack, Galvanic Corrosion, illustrated edition, (ASTM International: OH, USA, 1988).

13. N. Dai, L. Zhang, J. Zhang, Q. Chen, M. Wu, "Corrosion behaviour of selective laser melted Ti-6Al-4V alloy in NaCl solution", Corrosion Science, 102 (2016): 484-489.

African Corrosion Journal
Official publication of the Corrosion Institute of Southern Africa
www.africorr.org.za

Temporary coating for in process or storage applications

Markus Bieber
Cortec Corporation
4119 White Bear Parkway
St. Paul, MN 55110
USA

Dario Dell'Orto
Cortec Corporation
4119 White Bear Parkway
St. Paul, MN 55110
USA

ARTICLE INFO

Keywords:
Corrosion
Protection
Inhibitor
Temporary
Coating

ABSTRACT

There is a tremendous need for the protection of assets during processing, shipment and storage. Critical spares must be readily available and easy to place into service with minimal impact to the operation of equipment. The proven technology of VCIs (Vapor Corrosion Inhibitors) has long been used to preserve many of these assets using traditional mechanisms such as papers and films. Newer advances have allowed the use of this VCI technology to be incorporated into temporary coatings which are designed to provide corrosion protection in extreme environments, yet still be easy to remove compared to the older traditional wax type coatings or permanent coatings. By incorporating the VCI technology into these temporary coatings, it allows the use of thinner film thicknesses and less reliance on a thick barrier to keep contaminants away from the surface[1,2].

1. Introduction

Four Learning Objectives

What is a VCI?

VCI (Vapor Corrosion Inhibitor) is a corrosion inhibiting technology which consists of various organic and inorganic compounds which have an attraction to a metal surface. When properly formulated and compounded, this technology can be used in a multitude of carrier systems, such as coatings, which bring the inhibitors close to the metal substrate.

How VCIs work in a coating

VCIs are formulated into a coating by a complex development process which involves determining chemical compatibility of the VCIs with the other components of the coating such as the resin, solvents, pigments and other additives used for a variety of reasons. VCIs work by adsorbing onto the metal surface in a non-reactive attractive capacity, i.e., they are attracted to the metal through the particle charge[3].

How VCIs compare to traditional inhibitors

VCIs compare with traditional inhibitor systems by using smaller particles, as well as relying not only on contact inhibition but also vapor phase inhibition, thus providing more complete coverage and protection of the surface. This is illustrated in Figure 1.

The larger platelets are representative of traditional inhibitors which are unable to fill the micro-crevices, leaving gaps where corrosion can start and/or grow[4].

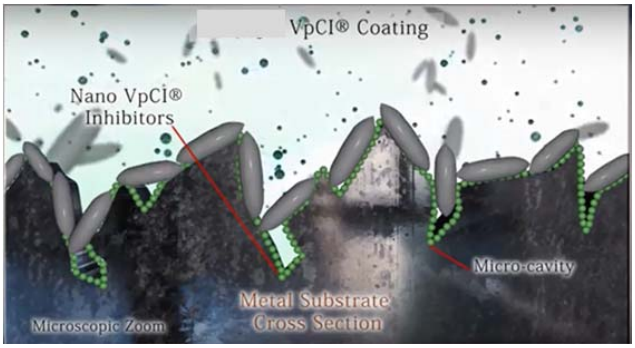

Figure 1: Schematic Diagram of a VCI Coating

What type of coating systems can use VCIs?

VCIs can be used with most coating systems. There are many variations of VCIs and it is necessary to choose the correct VCI for the corresponding coating system by checking compatibility, effectiveness and processability.

The environmental advantages of VCIs over traditional inhibitors

Traditional inhibitors containing heavy metals are becoming increasingly more regulated and often are no longer allowed to be used due to the negative impact they have on the environment and carcinogenic effects on workers exposed to them[5]. The environmental advantages of using VCIs are that they are non-toxic, do not contain heavy metals, and have no adverse effect due to their low usage concentrations. VCIs have long been used in other products such as PE films, foams, powders and liquids to provide a vapor phase of corrosion protection without impacting the environment[6,7,8,9].

2. Experimental Procedures

These studies examined the effectiveness of various types of corrosion inhibitors in solvent and waterborne removable coatings, based on salt fog results, (ASTM B117) and humidity results (ASTM D1748).

Each coating was applied on cold rolled steel (CRS) panels (SAE 1010), or on actual parts provided by customers. Dry film thicknesses (DFTs) were according to manufacturers' recommendations.

3 Results

Salt spray and humidity chamber tests are considered industry standards for corrosion testing. As shown by Figures 2-6 below, the difference in corrosion protection with VCI added is quite noticeable. The differences are noted below.

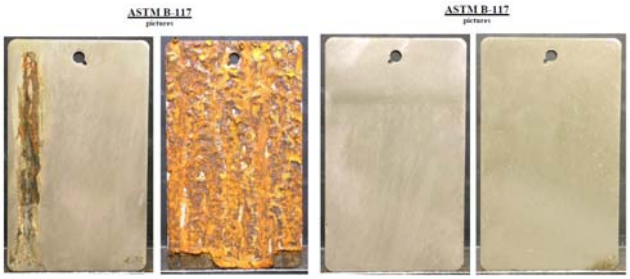

Sample A 350 Hours Without VCI	Sample B 50 Hours Without VCI	Sample A 400 Hours With VCI	Sample B > 400 Hours With VCI

Figure 2: Salt Spray Testing for competitive solvent-borne wax type coating with and without VCI inhibitors

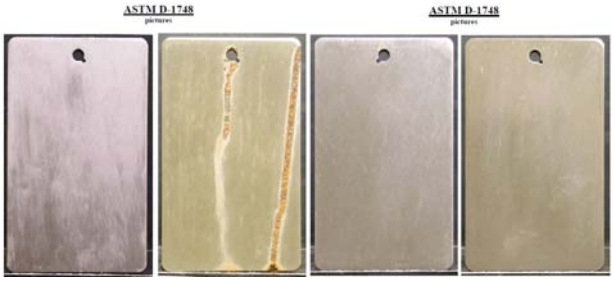

Sample A 3170 Hours Without VCI	Sample B 1100 Hours Without VCI	Sample A >3170 Hours With VCI	Sample B >3170 Hours With VCI

Figure 3: Humidity Testing for competitive solvent-borne wax type coating with and without VCI inhibitors

Sample A Solvent-borne Coating without VCI	Sample B Solvent-borne Coating with VCI	Sample C Waterborne Coating with VCI

Figure 4: Salt Spray (ASTM B117) Testing for Various Systems (600 hours)

VCI Coating Non-VCI Coating

Figure 5: Self- Healing Effect of the VCI on the Scribe in Salt Spray Testing

Figure 6: Humidity Testing for solvent-borne wax type coating and waterborne wax type coating with VCI inhibitors (768 hours)

This testing shows that waterborne systems can compete with solvent-borne systems by the use of VCI inhibitors. However, there are some distinct advantages of using a waterborne system which include:

- More Environmentally friendly
- Lower VOCs
- Easier cleanup

4 Examples of Other Technologies Using VCI Inhibitors

Film Using Inferior Inhibitors Film Using VCI Inhibitors

Figure 7: Engine Components Packaging in VCI film

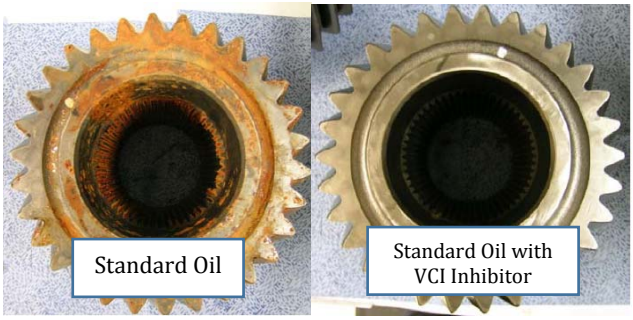

Preservative without Inhibitors Preservative with VCI Inhibitors

Figure 8: Transmission Components in Preservative Oils

5 Case History 1

5.1 Problem

A manufacturer of large construction graders needed an effective alternative to prevent corrosion on their products. There were several disadvantages to the heavy wax type product they were using. First, it did not always work if the equipment was stored outdoors for extended periods of time before shipping. Secondly, it left a greasy and slippery film on the graders, which made it difficult to climb into them for moving and shipping. Finally, the product was hard to remove and had to be disposed of as hazardous waste.

5.2 Application

The manufacturer sprayed the VCI containing coating and solvent in a 3:1 ratio on the equipment, which resulted in dry coat thicknesses between 0.8 and 1 mil (20- 25microns). Then the machines were transported by rail to the seaports. A few of the graders were placed in containers, but most were left uncovered.

The VCI containing coating at 1mil (25 microns) outperformed the heavy wax type coating at 3 mil (75 microns). The manufacturer also found the VCI containing coating easier to spray, free of offensive odors and much easier to remove. After two years of export shipments, they had experienced no corrosion problems when using the thinner film VCI containing coating.

6 Case History 2

6.1 Problem

A manufacturer of industrial equipment was struggling with protecting critically machined surfaces from corrosion and damage during transport. Due to the nature of the equipment, they were not able to deal with spray applying a coating, nor washing it down for removal.

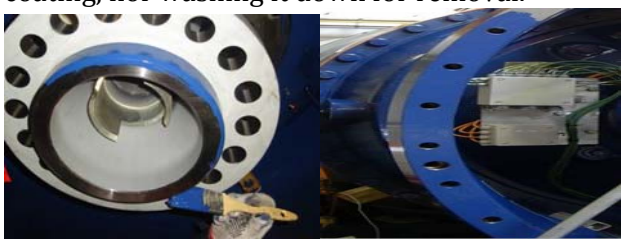

5.2 Application

The manufacturer brush applied the waterborne VCI containing coating onto the equipment, which resulted in dry coat thicknesses between 2-10 mil (50- 250 microns). The equipment was transport to the final destination where the coating was removed by simply peeling it off.

4. Conclusions

With corrosion costs in the billions of dollars and making up as much as 3% of USA's GDP[10], there is a need in the market place, for environmentally friendly, low VOC, removable coatings that can be applied at a thin film thickness (1.0 mils) which provide excellent corrosion protection and yet can still be easily removed. Compared to permanent coatings where removal requires blasting or the use of heavy duty solvents, or thick heavy barrier type wax coatings which are difficult to remove and dispose of, many removable thin film coatings with VCI technology can be easily removed using an alkaline solution and high pressure water.

By research, this paper shows that systems enhanced with VCI inhibitors can greatly improve the corrosion resistance of both solvent and waterborne coatings. In addition, waterborne coatings with VCI inhibitors can compete from a performance aspect with solvent-borne systems, while at the same time being more environmentally friendly, easier to cleanup and lower in VOCs.

References

1. C.W, Lea, FUCHS Lubricants, 2003 National Corrosion Service.

2. S. Prabhu, "Temporary Corrosion Protection during Storage, Transportation and Handling" (2016).

3. B.A., Miksic, "Use of Vapor Phase Inhibitors for Corrosion Protection of Metal Products," CORROSION/83 paper no.308 (Houston, TX: NACE, 1983).

4. Y.I., Kuznetsov,, "Inhibiting Action and Absorption of Beta-Aminoketones on Metals", Zasshchita Metallov, 32, 5 (1996) pp. 528-533.

5. Technical Rules for Hazardous Substances, "TRGS 615", (2007).

6. 48-hour Static Acute D. pulex Water Accomodating Fraction (WAF) Toxicity Testing, Environmental Enterprises USA, Inc., March 1, 2017

7. 96-hour Static Acute P. Promelas Water Accomodating Fraction (WAF) Toxicity Testing, Environmental Enterprises USA, Inc., March 1, 2017

8. 48-HourStatic Acute Seawater, A-bahia Water Accomodating Fraction (WAF) Toxicity Testing, Environmental Enterprises USA, Inc., March 1, 2017

9. 96-hour Static Acute Seawater, M.beryllina Water Accomodating Fraction (WAF) Toxicity Testing, Environmental Enterprises USA, Inc., March 1, 2017

10. NACE, "Cost of Corrosion Study," (2002).

African Corrosion Journal
Official publication of the Corrosion Institute of Southern Africa
www.africorr.org.za

Corrosion characterization of ruthenium implanted AISI 304L in proton exchange membrane fuel cell environments

Fortunate Moyo
University of the Witwatersrand
1 Jam Smuts
Johannesburg 2050
South Africa

Josias van der Merwe
University of the Witwatersrand
1 Jan Smuts
Johannesburg 2050
South Africa

Daniel Wamwangi
University of the Witwatersrand
1 Jan Smuts
Johannesburg 2050
South Africa

ARTICLE INFO

Keywords:
Corrosion
Ruthenium
Proton exchange membrane fuel cells
Ion implantation

ABSTRACT

Ruthenium was implanted into 304L stainless steel to increase corrosion resistance in a synthetic proton exchange membrane fuel cells (PEMFCs) simulation solution consisting of 10^{-4} M H_2SO_4 and 0.5 M sodium sulfate (Na_2SO_4) at 60°C. Corrosion characterization was done using potentiodynamic and potentiostatic measurement techniques, and metallic contaminants in the corrosion medium were measured using atomic absorption spectroscopy. Potentiostatic polarization was done at potentials typical of the anode and cathode environments of PEMFCs, with immersion times of up to 10 days. The corrosion rate of the ruthenium implanted stainless steel was <16 μA/cm², the target corrosion rate for PEMFCs. The treated stainless steel exhibited long term electrochemical stability in the simulated PEMFC environments. Metal dissolution at 645 $mV_{Ag/AgCl}$ decreased by ≈ 35% after implantation, indicating the suitability of ruthenium implanted stainless steel in the cathode environment of PEMFCs.

1. Introduction

Fuel cells are an environmentally benign source of energy because they generate electricity through electrochemical reactions, rather than combustion. Presently, fuel cells are largely used as stationary power generators at hospitals, hotels, schools, office buildings and airport terminals.[1] However, their largest application is potentially in transportation, which contributes 23 to 24% of the world's greenhouse emissions.[2,3] In the face of increasing crude oil prices, diminishing fuel reserves and mounting pressure to reduce the global carbon footprint, fuel cells present an attractive alternative source of energy for automotive applications.

Proton exchange membrane fuel cells (PEMFCs) in particular, hold significant promise for transport applications. They have low operating temperatures, low noise, quick start-up capability and high power density.[4,5] Crucial components of PEMFCs are bipolar plates (Figure 1), whose functions include: (1) separating the air (oxygen) and the fuel (hydrogen), (2) providing mechanical support and strength to the fuel cell assembly, (3) conducting electrical output, (4) moderating the temperature of the cell, which is typically between

60 and 80 °C, and (5) distributing fuel gas and air.[6-8]

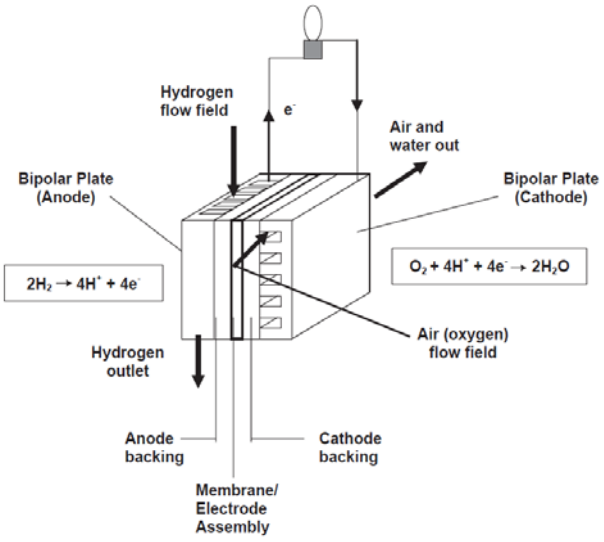

Figure 1: Schematic diagram of a PEMFC.[6]

The multifunctional characteristic of bipolar plates requires a material with an assortment of properties, including good thermal and electrical conductivity, high strength, good machinability and most importantly, zero permeability to the reactant gases used in PEMFCs. Stainless steels such as AISI 304L easily satisfy these requirements. Furthermore, the wide availability of stainless steels presents an opportunity for cost effective mass production of PEMFCs.

However, stainless steels are prone to corrosion in the reducing acidic conditions generated in PEMFCs.[7,8] Reactions at the anode (Figure 1) involve the oxidation of hydrogen, Equation 1, and the ions thus produced are reduced at the cathode according to Equation 2.[6,9] Corrosion of stainless steel bipolar plates deteriorates the performance of PEMFCs because corrosion products increase interfacial contact resistance between the plates and reduce power output. In addition, dissolved metallic ions poison the catalyst in the polymeric membrane,[10,11] further reducing cell efficiency by lowering ionic conductivity of the membrane and increasing charge transfer resistance.

$$2H_2 \rightarrow 4H^+ + 4\bar{e} \qquad \text{(Equation 1)}$$

$$2O_2 + 4H^+ + 4\bar{e} \rightarrow 2H_2O \qquad \text{(Equation 2)}$$

Surface modification is undoubtedly a cost effective means of improving corrosion resistance of stainless steels in PEMFCs environments. Several researchers have focused on coating stainless steels with protective layers of titanium nitride,[12-14] chromium-carbon[15,16] and carbon[17] produced mostly by physical vapor deposition. Although some of the coatings studied exhibited metal-like electrical conductivity and/or adequately inhibited metal dissolution, there are still concerns around intrinsic defects such as pinholes and poor adhesion. These defects make long-term applicability of the coatings in PEMFCs doubtful, and necessitate consideration of alternative surface modification techniques.

In this study, ruthenium was implanted into 304L stainless steel and the effect on corrosion resistance in PEMFC simulated environments was investigated. Ion implantation is largely used for doping semiconductors for electronic application, but has attracted substantial interest in the field of corrosion in recent years,[18-23] and has been considered for application in PEMFCs.[24,25] Implanted Ru was demonstrated by Tjong and Chu[22] to improve corrosion resistance of ferritic stainless steel in 0.5 M sulfuric acid (H_2SO_4), and could potentially be beneficial in PEMFCs.

2. Experimental Procedure

Samples of AISI 304L stainless steel (18.32 Cr, 8.20 Ni (wt%)) measuring 20 x 20 mm^2 were cut from a 6 mm thick plate and mechanically ground with a series of silicon carbide papers of decreasing grit size to a finish of 120 grit (~125 µm). The samples were then cleaned ultrasonically: first with detergent water and then with ethanol for 20 minutes to remove any embedded silicon carbide particles and other contaminants due to sample handling.

Thereafter, the 304L stainless steel samples were implanted at room temperature with 50 keV Ru ions in a Varian 350D ion implanter using a dose of $1x10^{16}$ ions/cm^2 at a zero degree angle. Simulation of the implantation process using Stopping Range of Ions in Matter (SRIM) and $90x10^3$ ions revealed that the peak concentration of Ru should lie 13 nm beneath the stainless steel surface.

To analyze and confirm Ru distribution in the stainless steel, Rutherford Backscattering Spectroscopy (RBS) was carried out using 3.6 MeV helium ions with a spot size of 500 x 500 μm^2. The back scattered particles were detected with a solid-state detector located at 150° to the primary

ion beam, and the recorded spectra were simulated using the RUMP code.

An electrolyte consisting of 10^{-4} M H_2SO_4 and 0.5 M sodium sulfate (Na_2SO_4)[26] was used to simulate the PEMFC medium. Corrosion characterization was done at different potentials for periods ranging from 2 to 240 h: at the corrosion potential (E_{corr}), at -195 $mV_{Ag/AgCl}$ (-240 mV_{SCE}) the operation potential in simulated anode environments, and at 645 $mV_{Ag/AgCl}$ (600 mV_{SCE}) the operation potential in simulated cathodic environments.[12] Potentiodynamic polarization was done at a scan rate of 0.5 mV/s from cathodic to anodic potentials, and the recorded data were used to calculate current densities (i_{corr}) by the Stern-Geary method as described in ASTM G102-89 (2010).[27]

All electrochemical tests were done at 60 ± 1 °C in a thermally controlled 3-electrode electrochemical cell comprising the test sample as the working electrode, a Ag/AgCl reference electrode (~199 mV_{SHE}), and a large area graphite electrode. The reference electrode had an application range of 0-80 °C. A PGSTAT302 Autolab potentiostat interfaced with Nova 1.70 data acquisition software was used. The electrolyte used to simulate the PEMFC medium was highly conductive; hence, no potential drop (IR) compensation was done. Fresh solutions were used for every test, and pristine (non-implanted) 304L stainless steel was used as a control.

The chemical composition of the PEMFC synthetic solution was analyzed after corrosion exposure using an atomic absorption spectroscopy (AAS). Analysis was limited to iron and chromium ions, which can potentially contaminate the membrane and catalyst in PEMFCs.[10] In all instances, fresh solutions and deionized water were used as controls.

To guard against systematic errors, all tests were randomized. The precision of the potentiostat used in this study was determined as described elsewhere.[28,29] E_{corr} values measured by the potentiostat were accurate to within ± 7.4 mV, and i_{corr} values to within ± 7.1 μA/cm². Since the number of replicates per test condition was limited by financial constraints, it was assumed that the E_{corr} and i_{corr} measurements on the samples had similar precision and repeatability as the potentiostat.

3. Results

Figure 2 shows the RBS spectra obtained on the pristine and Ru implanted 304L stainless steel. In Figure 2(b), there is a distinct peak at ~3.1 MeV, corresponding to the implanted Ru.

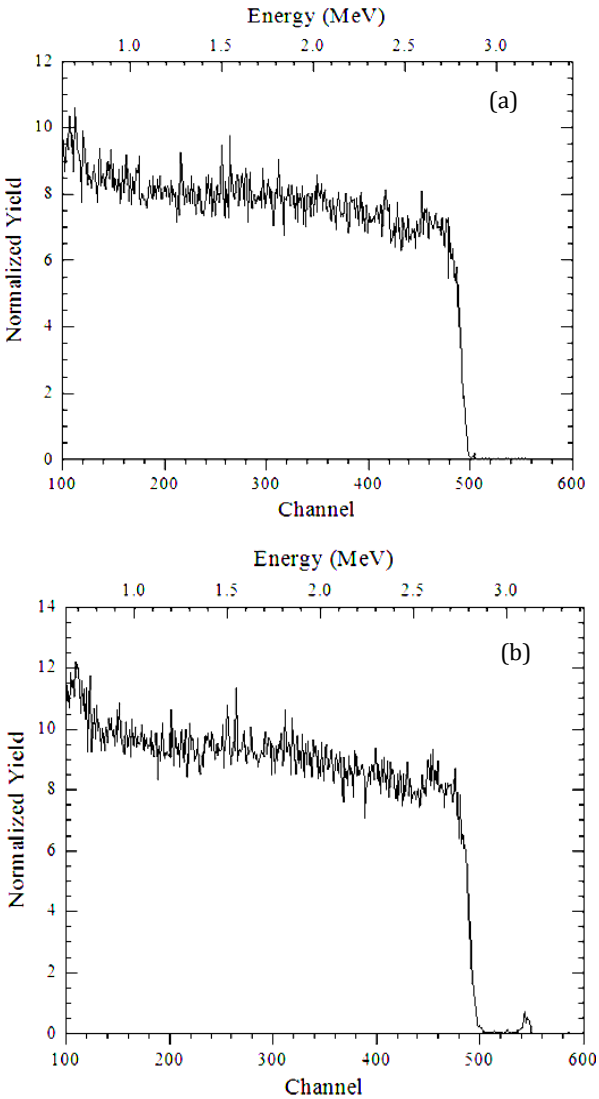

Figure 2: RBS spectra of (a) pristine and (b) Ru implanted 304L stainless steel after ion implantation at 50 keV using $1x10^6$ ions/cm².

Potentiodynamic polarization curves for pristine and Ru implanted 304L stainless steel in the simulated fuel cell solution are shown in Figure 3. On the whole, both specimens had corrosion rates that were < 16 μA/cm², the target corrosion rate for bipolar plates used in PEMFCs.[7] In fact, the

corrosion rates of the stainless steel before and after Ru implantation were similar: ~0.04 and 0.035 μA/cm^2 respectively.

Figure 3 shows a higher value of E_{corr} for the Ru implanted stainless steel. It was ~ -60 mV compared to ~ -160 mV for pristine 304L stainless steel. This rise in E_{corr} was likely a consequence of cathodic modification,[30,31] where Ru lowered the hydrogen overvoltage of 304L stainless steel, increased the efficiency of the cathodic corrosion reaction and shifted E_{corr} to more anodic values.

For both test samples, the E_{corr} was greater than -195 mV, the operation potential of the anode environment of PEMFCs. This means that both the pristine and Ru implanted 304L stainless steel would be corrosion resistant in the anode environment of the fuel cell. At potentials typical of the cathode environment of PEMFCs (~645 $mV_{Ag/AgCl}$), pristine 304L stainless steel could be susceptible to significant dissolution. It is clear from Figure 3 that these potentials coincided with the onset of transpassive corrosion of the stainless steel, where trivalent chromium responsible for passivity is oxidized to non-protective hexavalent Cr.

The curve corresponding to Ru implanted stainless steel clearly showed the absence of the anodic 'nose' typical of active-passive alloys. This implies that the implanted stainless steel was prone to spontaneous passivation in the simulated solution. The anodic 'nose' on the curve corresponding to pristine 304L stainless steel was very small but significantly wide, suggesting difficulty to passivate in the test solution.

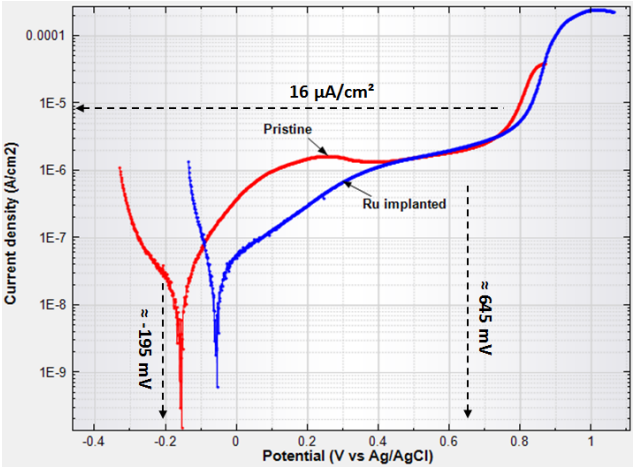

Figure 3: Polarization curves of pristine and Ru implanted 304L stainless steels after 24 h immersion in 10^{-4} M H_2SO_4 with 0.5 M Na_2SO_4 at 60°C, at a scan rate of 0.5 mV/s vs Ag/AgCl.

Figure 4 shows that results obtained when the test samples were exposed to the simulated fuel cell solution for 10 days. Open circuit potential (OCP) for both pristine and Ru implanted 304L stainless steel shifted towards positive potentials (Figure 4(a)). This is consistent with moving to potentials where Cr (III) species are predominant and thermodynamically stable,[32] and points to increased ability to form stable protective Cr (III) films with increase in exposure time.

Noticeably, OCP values on Ru implanted stainless steel were nearly steady, varying from ~100 to 140 mV in the last 8 days of exposure. For the same period, the OCP values recorded on the pristine 304L stainless steel ranged from ≈ 100 to 230 mV. This wide range in OCP could have been caused by a thickening passive layer, which is likely to increase interfacial contact resistance (ICR) of the fuel cell during operation and result in reduced cell efficiency.

The amount of iron dissolved during the 10 day exposure is presented in Figure 4(b). Introducing Ru via ion implantation clearly reduced susceptibility for the stainless steel to dissolution by > 50% in some instances. Nonetheless, the amount of dissolved iron in the corrosion solutions increased with increased exposure time, suggesting that with time, cell efficiency could potentially decrease due to poisoning of the catalyst in the polymeric membrane.

Current-time curves for pristine and Ru implanted 304L stainless steel at 645 and -195 $mV_{Ag/AgCl}$ are presented in Figure 5. For clarity, data > |1 μA/cm^2| were omitted from the analyses in the figure.

Current density values recorded on the pristine 304L stainless steel at 645 mV were quite erratic as can be seen in Figure 5(a). This is consistent with the expectation that 645 mV, the typical potential of PEMFC cathode environment, coincided with the onset of transpassive corrosion for the pristine stainless steel (Figure 3). Transpassive corrosion is typically characterized

by localized dissolution of Cr (III) films that presumably cover the stainless steel surface when it is passive, and this dissolution results in current transients, such as those observed in Figure 5(a). On the other hand, current densities on the Ru implanted 304L stainless steel were very stable over the same exposure period, and were mostly < 0.1 μA/cm^2. It is likely therefore that Ru implanted 304L stainless steel would be much more stable in the cathode region of the fuel cell than pristine stainless steel.

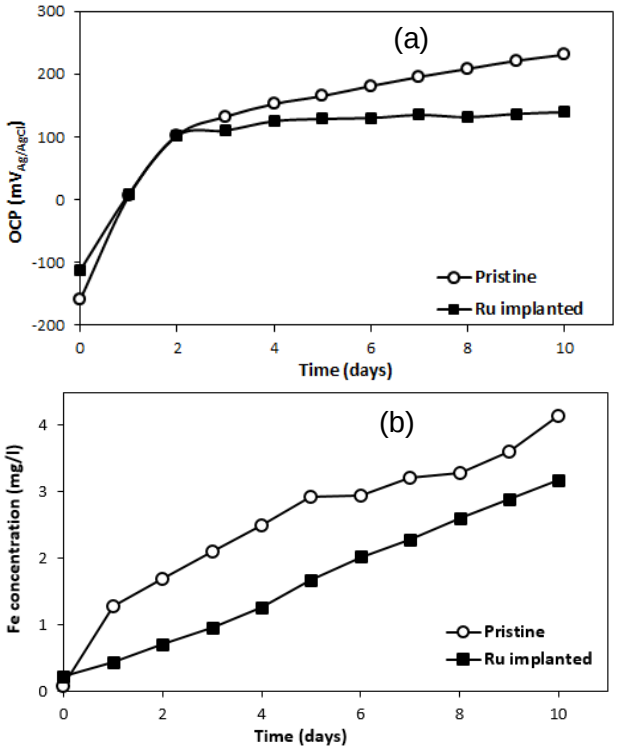

Figure 4: Variation of (a) OCP vs Ag/AgCl, and (b) dissolved iron with time for pristine and Ru implanted 304L stainless steel during exposure to 10^{-4} M H_2SO_4 with 0.5 M Na_2SO_4 at 60°C for 10 days.

At potentials typical of the PEFMC anode environment (~ -195 mV$_{Ag/AgCl}$), the current densities recorded on the two samples were negative (Figure 5(b)). Consistent with Figure 3, no metal dissolution would be expected from both the pristine and Ru implanted stainless steel at these potentials. The current densities recorded in Figure 5(b) are possibly associated with hydrogen evolution by Equation 3, which is a typical supporting cathodic reaction in corrosion occurring in acidic media. Current density values on the Ru implanted samples were numerically larger, suggesting higher reaction rates on the alloy surface. This is consistent with the principle of cathodic modification mentioned earlier.

$$2H^+ + 2\bar{e} \rightarrow H_2 \qquad \text{(Equation 3)}$$

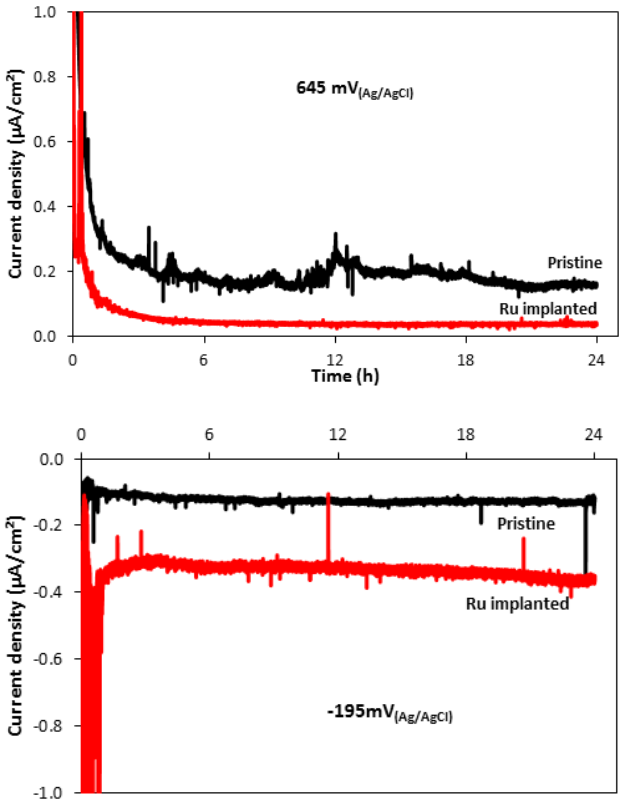

Figure 5: Current vs time plots for pristine and Ru implanted 304 stainless steel potentiostatically polarized in 10^{-4} M H_2SO_4 with 0.5 M Na_2SO_4 at 60°C for 24 h at: (a) 645 mV and (b) -195 mV vs Ag/AgCl.

After potentiostatic exposure at 645 mV, the chemical composition of the solution was analyzed via AAS, and the results obtained are given in Figure 6. The high iron dissolution associated with the pristine 304L stainless steel confirmed that metal dissolution would be higher as 645 mV coincided with the onset of transpassive corrosion. Interestingly, the amount of Cr dissolved during exposure was the same for both pristine and Ru implanted 304L stainless steels. It should be noted that the AAS used in this analysis had no capacity to distinguish Cr (III) and Cr (VI) ions.

4. Discussion

The corrosion resistance of 304L stainless steel relies on the formation of a self-healing tenacious Cr (III) oxide on its surface. Although generally protective, Cr_2O_3 films are prone to dissolution in

acidic media and at potentials > 800 mV_{SHE} (~600 $mV_{Ag/AgCl}$).[32] At this potential range, also known as the transpassive region, Cr (III) is oxidized to soluble Cr (VI) species such as CrO_4^{2-} and $Cr_2O_7^{2-}$, which are not protective.[33]

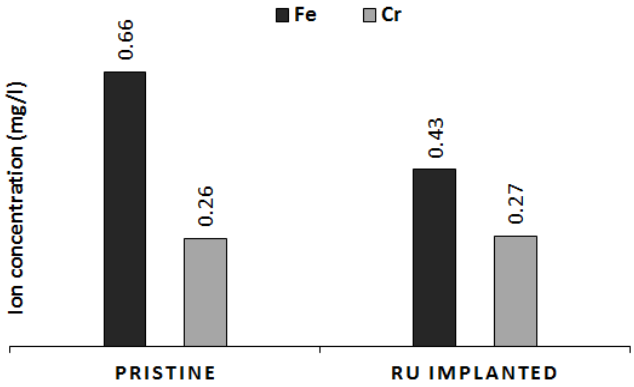

Figure 6: Concentration of iron and chromium dissolved from pristine and Ru implanted 304L after 24 h exposure to 10^{-4} M H_2SO_4 with 0.5 M Na_2SO_4 at 60°C and 645 mV vs Ag/AgCl.

As shown in Figure 3, the onset of transpassive corrosion for pristine 304L stainless steel exposed to 10^{-4} M H_2SO_4 with 0.5 M Na_2SO_4 occurred at ~650 mV, which coincided with the typical potential for the PEMFC cathode environment. Inevitably, 304L stainless steel would be prone to significant dissolution in this environment as demonstrated in Figure 6, which would in turn poison the catalyst in the polymeric membrane.

Adding Ru to the surface of 304L stainless steel via ion implantation seemed to increase the tolerance of the stainless steel in the fuel cell simulation solution by shifting the onset of transpassive potentials to higher values. The lower iron dissolution and steady current variations in Figures 6 and 5(a) confirmed this supposition. Ru had the effect of increasing the rate of hydrogen evolution by Equation 3, and shifting E_{corr} to more anodic potentials as demonstrated in Figures 3 and 5(b) and by previous researchers in acidic media.[22,34,35] However, there is no documentation to support the shift in transpassive potentials observed in Figure 3, implying that an additional mechanism of corrosion protection occurred.

Ion implantation is a process known to create nearly amorphic surface layers.[18,36] Transpassive corrosion is typically intergranular, consistent with the fact that grain boundaries are high energy regions, and are easily prone to anodic dissolution. Amorphisation therefore reduces tendency to undergo intergranular attack, and could potentially increase resistance of 304L stainless steel to dissolution at ~645 $mV_{Ag/AgCl}$.

The OCP of pristine 304L stainless steel in 10^{-4} M H_2SO_4 with 0.5 M Na_2SO_4 markedly increased during exposure (Figure 4(a)). Decreasing OCP values are typically associated with dissolving or thinning passive films,[37,38] and similarly, increasing OCP values indicate thickening passive films. Considering that passive films are essentially products of corrosion, thick passive films could indicate large amounts of corrosion products on the stainless steel surface, which could significantly increase ICR of the PEMFCs and reduce cell efficiency.

In the presence of Ru, OCP variations on 304L stainless were relatively steadier throughout the analysis period (Figure 4(a)) indicating passive films of nearly constant thickness. In addition, measured OCP values were mainly lower than those recorded on pristine 304L stainless steel. This suggests the formation of thinner passive films and accumulation of less corrosion product on the metal surface, which could result in lower ICR and better cell efficiency. Reduced metal dissolution reported in Figures 4(b) and 6 demonstrated the protectiveness of these films.

5. Conclusions

The corrosion behavior of Ru implanted 304L stainless steel was characterized in 10^{-4} M H_2SO_4 with 0.5 M Na_2SO_4 at 60°C with the view of potential application in PEMFCs. Although the presence of implanted Ru did not necessarily result in lower corrosion rates, it certainly increased tolerance of 304L stainless steel in the cathode environment of PEMFCs (~645 $mV_{Ag/AgCl}$) by shifting transpassive potentials to higher values. Long term, Ru implanted stainless steel exhibited stable performance, which is essential for long term stability of PEMFCs.

While the results of this study show that Ru implanted stainless steel holds promise for

potential as-cast application in PEMFCs as bipolar plates, it is necessary to:

1. optimize Ru implantation dose to maximize performance
2. investigate ICR of the Ru implanted stainless steel.

Acknowledgements

The support of DST-NRF Centre of Excellence in Strong Materials (CoE-SM) towards this research is hereby acknowledged. The Department of Science and Technology, and National Research Foundation, South Africa are thanked for financial support. The authors are grateful to Anglo Platinum for providing the powder used to prepare the ruthenium target used in ion implantation. Many thanks to iThemba LABS (North) for generously allowing the authors access to the ion implanter.

References

1. A. Sakhare, A. Davari, A. Feliachi, "Fuzzy logic control of fuel cell for stand-alone and grid connection," *Journal of Power Sources* 13 (2004): pp. 165-176.

2. W. Rothengatter, "Climate change and the contribution of transport: Basic facts and the role of aviation," *Transportation Research Part D* 15 (2010): pp. 5-13.

3. R. Sims, R. Schaeffer, F. Creutzig, X. Cruz-Núñez, M. D'Agosto, D. Dimitriu, M.J. Figueroa Meza, L. Fulton, S. Kobayashi, O. Lah, A. McKinnon, P. Newman, M. Ouyang, J.J. Schauer, D. Sperling, and G. Tiwari, "Transport," IPCC Climate Change 2014: Mitigation of Climate Change. Contribution of working group III to the Fifth Assessment Report of the Intergovernmental Panel on Climate Change [Edenhofer, O., R. Pichs-Madruga, Y. Sokona, E. Farahani, S. Kadner, K. Seyboth, A. Adler, I. Baum, S. Brunner, P. Eickemeier, B. Kriemann, J. Savolainen, S. Schlömer, C. von Stechow, T. Zwickel and J.C. Minx (eds.)] (Cambridge, UK, New York, USA: Cambridge University Press, 2014), p. 603.

4. C. Wang, S. Wang, L. Peng, J. Zhang, Z. Shao, J. Huang, C. Sun, M. Ouyan, X. He, "Recent progress on the key materials and components for proton exchange membrane fuel cells in vehicle applications," *Energies* 9, 603 (2016): pp. 1-39.

5. W.R.W. Daud, R.E. Rosli, E.H. Majlan, S.A.A. Hamid, R. Mohamed, T. Husaini, "PEM fuel cell system control: A review," *Renewable Energy* 113 (2017): pp. 620-638.

6. A. Hermann, T. Chaudhuri, P. Spagnol, "Bipolar plates for PEM fuel cells: A review," *International Journal of Hydrogen Energy* 30 (2005): pp. 1297-1302.

7. D.J.L. Brett, N.P. Brandon, "Review of materials and characterization methods for polymer electrolyte

fuel cell flow-field plates," *Journal of Fuel Cell Science and Technology* 4 (2007): pp. 29-44.

8. R.A. Antunes, M.C.L. Oliveria, G. Ett, V. Ett, "Corrosion of metal bipolar plates for PEM fuel cells: A review," *International Journal of Hydrogen Energy* 35 (2010): pp. 3632-3647.

9. S.-J. Lee, C.-H. Haung, J.-J. Lai, Y.-P. Chen, "Corrosion-resistant component for PEM fuel cells," *Journal of Power Sources* 131 (2004): pp. 162-168.

10. A. Pozio, R.F. Silva, M. De Francesco, L. Giorgi, "Nafion degradation in PEFCs from end plate iron contamination," *Electrochimica Acta* 48 (2003): pp. 1543-1549.

11. P. Ju, Y. Zuo, Y. Tang, X. Zhao, "The enhanced passivation of 316L stainless steel in a simulated fuel cell environment by surface plating with palladium," *Corrosion Science* 66 (2013): pp. 330-336.

12. M. Li, S. Luo, C. Zeng, J. Shen, H. Liu, C. Cao, "Corrosion behavior of TiN coated type 316 stainless steel in simulated PEMFC environments," *Corrosion Science* 46 (2004): pp. 1369-1380.

13. E.A. Cho, U.-S. Jeon, S.-A. Hong, I.-H. Oh, S.-G. Kang, "Performance of a 1 kW-class PEMFC stack using TiN-coated 316 stainless steel bipolar plates," *Journal of Power Sources* 142 (2005): pp. 177-183.

14. Y. Wang, D.O. Northwood, "An investigation into TiN-coated 316L stainless steel as a bipolar plate material for PEM fuel cell," *Journal of Power Sources* 165 (2007): pp. 293-298.

15. H.-C. Wang, H.-H. Shen, C.-E. Lu, K.-H. Hou, M.-D. Ger, "Preparation of corrosion-resistant and conductive trivalent Cr-C coatings on 304 stainless steel for use as bipolar plates in proton exchange membrane fuel cells by electrodeposition," *Journal of Power Sources* 293 (2015): pp. 475-483.

16. W. Mingee, L. Congda, H. Tao, C. Guohai, W. Doughui, Z. Haifeng, Z. Doug, W. Aiying, "Chromium interlayer amorphous carbon film for 304 stainless steel bipolar plate for proton exchange membrane fuel cell," *Surface and Coatings Technology* 307 (2016): pp. 374-381.

17. T. Fukutsuka, T. Yamaguchi, S.-I. Miyano, Y. Matsuo, Y. Sugie, Z. Ogumi, "Carbon-coated stainless steel as PEFC bipolar plate material," *Journal of Power Sources* 174 (2007): pp. 199-205.

18. S.C. Tjong, M.C. Wong, S.P. Wong, "Corrosion behavior of boron- and phosphorous-implanted Fe-40Cr alloy in reducing acid solutions," *Applied Surface Science* 64 (1993): pp. 127-132.

19. M. Wang, Q.Y. Zhnag, W.D. Shi, T.C. Ma, S.Z. Hou, "Effects of Mo and Mo + N implantation on corrosion resistance of austenitic stainless steel," *Surface and Coatings Technology* 65 (1994): pp. 171-174.

20. C.M. Abreu, M.J. Cristóbal, X.R. Nóvoa, G. Pena, M.C. Pérez, R.J. Rodríguez, "Modifications of the stainless steel passive film induced by cerium implantation," *Surface and Coatings Technology* 158-159 (2002): pp. 582-587.

21. C.M. Abreu, M.J. Cristóbal, P. Merino, X.R. Nóvoa, G. Pena, M.C. Pérez, "Electrochemical behavior of an AISI 304L stainless steel implanted with nitrogen," *Electrochimica Acta* 53 (2008): pp. 6000-6007.

22. S.C. Tjong, P.K. Chu, "Corrosion properties of Fe-24Cr stainless steel alloy modified by plasma immersion ion implantation in 0.5 M sulfuric acid solution," *Surface and Coatings Technology* 201 (2007): pp. 6781-6784.

23. N. Padhy, S. Ningshen, B.K. Panigrahi, U.K. Mudali, "Corrosion behavior of nitrogen ion implanted AISI type 304L stainless steel in nitric acid medium," *Corrosion Science* 52 (2010): pp. 104-112.

24. K. Feng, Y. Sheu, J. Mai, D. Liu, X. Cai, " An investigation into nickel implanted 316L stainless steel as a bipolar plate for PEM fuel cell," *Journal of Power Sources* 182 (2008): pp. 145-152.

25. K. Feng, Y. Sheu, D. Liu, P.K. Chu, X. Cai, "Ni-Cr Co-implanted 316L stainless steel as bipolar plate in polymer electrolyte membrane fuel cells," *International Journal of Hydrogen Energy* 35 (2010): pp. 690-700.

26. J.S. Kim, W.H.A. Peelen, K. Hemmes, R.C. Makkus, "Effects of alloying elements on the contact resistance and the passivation behavior of stainless steels," *Corrosion Science* 44 (2002): pp. 635-655.

27. ASTM G102-89 (2010), "Standard practice for calculating of corrosion rates and related information from electrochemical measurements" (West Conshohocken, PA: ASTM)

28. F. Moyo, J.W. van der Merwe, D. Wamwangi, "Corrosion performance of pulse plated ruthenium: Dependence on pulse-off time," *Surface and Coatings Technology* 307 (2016): pp. 971-977.

29. ASTM G16-95 (2010), "Standard guide for applying statistics to analysis of corrosion data" (West Conshohocken, PA: ASTM)

30. N.D. Tomashov, "Passivity and corrosion resistance of metal systems," *Corrosion Science* 4 (1964): pp. 315-334.

31. J.H. Potgieter, "Alloys cathodically modified with noble metals," *Journal of Applied Electrochemistry* 21 (1991): pp. 471-482.

32. S. Haupt, H.-H. Strehblow, "A combined surface analytical and electrochemical study of the formation of passive layers on Fe/Cr alloys in 0.5 M H_2SO_4," *Corrosion Science* 37(1) (1995): pp. 43-54.

33. P. Schmuki, "Form Bacon to barriers: a review on the passivity of metals and alloys," *Journal of Solid State Electrochemistry* 6 (2002): pp. 145-164.

34. E.M. Sherif, J.H. Potgieter, L. Cornish, P.A. Olubambi, C.N. Machio, "Effects of minor additions of ruthenium on the passivation of duplex stainless steel corrosion in concentrated hydrochloric acid solution," *Journal of Applied Electrochemistry* 39 (2009): pp. 1385-1392.

35. J.H. Potgieter, W.O. Barnard, G. Myburg, K. Varga, P. Baradlai, L. Tomcsanyi, "Corrosion behavior of duplex stainless steels containing minor ruthenium additions in reducing acid media," *Journal of Applied Electrochemistry* 26 (1996): pp. 1103-1110.

36. T.R. Rautray, R. Narayanau, K.-H. Kim, "Ion implantation of titanium based biomaterials," *Progress in Materials Science* 56 (2011): pp. 1137-1177.

37. E.M. Sherif, J.H. Potgieter, J.D. Comins, L. Cornish, P.A. Olubambi, C.N. Machio, "The beneficial effect of ruthenium additions on the passivation of duplex stainless steel corrosion in sodium chloride solution," *Corrosion Science* 51 (2009): pp. 1364-1371.

38. H. Luo, H. Su, B. Li, G. Ying, " Electrochemical and passive behavior of tin alloyed ferritic stainless steel in concrete environment," *Applied Surface Science* 439 (2018) pp. 232-239.

African Corrosion Journal
Official publication of the Corrosion Institute of Southern Africa
www.africorr.org.za

The effect of SiC content on the corrosion and tribocorrosion performance of SPS produced Al-SiC nanocomposites

P.V. Cobbinah
Vaal University of Technology
Department of Metallurgical Engineering
Andries Potgieter Blvd
Vanderbijlpark, Gauteng, 1911
South Africa

W.R. Matizamhuka
Vaal University of Technology
Department of Metallurgical Engineering
Andries Potgieter Blvd
Vanderbijlpark, Gauteng, 1911
South Africa

ARTICLE INFO

Keywords:
Spark plasma sintering (SPS)
Anodic and cathodic polarisation
Current density
Linear sweep voltammetry (LSV)
Tribocorrosion

ABSTRACT

Using the spark plasma sintering (SPS) technique, five Al-SiC composites were produced with differing proportions of SiC ranging from 15wt% to 40wt%. The relative densities of the SPS composites were above 97%, including for the Al alloy. Increasing the SiC content increased the hardness of the composites. The corrosion behaviour of the SPS Al-SiC composites immersed in 3.5wt% NaCl at room temperature were studied electrochemically by potentiodynamic polarisation. The Tafel polarisation plots showed that the corrosion resistance of composites reinforced with 15 and 20wt% SiC improved compared to the Al alloy. In all samples, pits were also observed on both the Al alloy and composites after polarisation. The synergistic effects of wear and corrosion on the composites were also assessed.

1. Introduction

Good corrosion resistance, superior wear resistance, lower coefficient of thermal expansion (CTE), improvements in both mechanical properties and structural efficiency are properties ascribed to metal matrix composites (MMCs).[1] Researchers have studied the mechanical and physical properties of aluminium MMCs [2–5] and also their corrosion behaviour.[6–8]

Although Al alloys are known to form a passive film[9], interactions between the reinforcing phase such as SiC and the monolithic Al alloy inevitably make the composite prone to corrosion. Metallurgical factors in the matrix, such as defects and composition inhomogeneities, contribute to corrosion of the composite, and these can serve as susceptible sites for the initiation of corrosion. At their interfaces, localised forms of corrosion, such as preferential or crevice attack and microgalvanic set-ups promote the degradation of the composites.[10,11]

Corrosion characteristics of Al-SiC composites are influenced by the volume fractions of the reinforcing phase.[12–14] Conversely, findings of other investigators[7,8,15] suggest the corrosion behaviour of the composite is independent of the amount of SiC making up the composite. The difference in findings can be as a result of the different processing routes[16], which influence the microstructures, and Al alloys[17] employed as matrix. However, despite the disagreement, all the investigators observed the formation of pits in both the composites and unreinforced matrix.

The phenomenon of tribocorrosion is the permanent deterioration of a material, resulting from simultaneous mechanical and chemical surface interactions existing in tribological contact in a corrosive environment. In a tribological system, the nature of wear, friction and lubrication influence tribocorrosion. Thus, the total material loss includes degradation from wear only, corrosion only and synergistic effects.[18] In general, as desired from composites, MMCs boast of a good balance of properties in relation to the individual inherent properties of the materials that make up the composite. In this respect, the addition of SiC to the Al alloy is to improve its wear properties with the aim of not losing its inherent corrosion resistance.

The study was on the corrosion behaviour of Al-SiC composites produced using spark plasma sintering (SPS). Not only is this method of fabrication energy efficient, it also achieves consolidation and homogenisation in a short time through volumetric joule heating of the samples aided by pressure leading to no grain growth.[19] Potentiodynamic polarisation was used to monitor the response of the composites to marine environments, and their corrosion resistance were subsequently assessed. The tribocorrosion performance of the composites were also studied.

2. Experimental Procedure

2.1. Materials and Sample Preparation

As-received powders include aluminium (99.5% purity, 7-15µm) and silicon carbide (SiC) (99% purity, 44µm). Composites reinforced with SiC ranging from 15 to 40 wt% were prepared. Using alumina balls, ball-to-powder ratio (BPR) of 5:1, a Reeves attritor mill and a rotating speed of 400 rpm, SiC was first wet milled in hexane for 16.5 hours and the Al alloy for 8 hours. The respective composites were also wet milled for 8 hours each and 2 wt% of polyethylene glycol (PEG) was added as a process control agent (PCA). The composites were then dried using a rotary evaporator. The PCA was burnt off in a tube furnace, under an argon atmosphere, at 400°C using a heating rate of 5°C/min and an isothermal hold time of 30mins. Spark plasma sintering (SPS) was carried out on each composite using a FCT HP-D5 sintering furnace at a pressure of 50MPa, a heating and cooling rate of 200°C/min and 100°C/min respectively. Samples were sintered at 600°C and held for 10mins in a vacuum. A graphite die of inner diameter 20mm and graphite punches were used. The die was lined with graphite foil along the cylindrical surface and at the flat ends, and hexagonal boron nitride (hBN) coated graphite foils were used.

2.2. Powder and Composite Characterisation

Using a Malversizer, the particle size distribution of the as-received powders (Al alloy and SiC) and milled powders were analysed before sintering. For metallography, sintered composites were ground with SiC paper through to 1200 grit, polished with diamond paste suspensions up to 1µm and etched with Keller's reagent. Phase identification and morphological studies of composites were carried out using a Shimadzu XRD-7000 diffractometer and an Olympus BX51M optical microscope. A Carl Zeiss Sigma field emission SEM was used to determine the composition of the various microstructural features.

2.3. Density and Hardness Determination

Sintered samples were sand blasted to remove the attached coating and graphite foil. Using Archimedes' principle to calculate the actual density in Equation 1, sintered samples were first weighed in air (W_α) and after weighed again while suspended in distilled water (W_w).

$$\rho_a = \left(\frac{W_\alpha}{W_\alpha - W_w}\right) X\ \rho_b \qquad (1)$$

where ρ_a = actual density, W_α = mass of the sample in air, W_w = mass in distilled water and ρ_w = density of distilled water.

Hardness testing was carried out using an Innovast Falcon 500 by subjecting the sintered composites to a load of 5N for 10 seconds for seven different indentations.

2.4. Electrochemical Corrosion Testing

Sintered samples for corrosion testing were cut into dimensions of 10mm X 10mm. With an

aluminium tape, an electrical wire was attached to the surface of each cut sample which was then mounted. The 1cm² exposed surface were then ground to 1200 grit, rinsed with ethanol, hot air dried and kept in a desiccator. The mounted samples with the wire protrusion served as the working electrode, an Ag/AgCl electrode was used as the reference electrode and platinum wire as the counter electrode. Using the Digi-Ivy potentiostat and DY2300 series software, the exposed surfaces were immersed in 3.5wt% NaCl solution and polarised.

The corrosion behaviour of the composites were assessed from the Tafel polarization plots obtained by linear sweep voltammetry (LSV) test, at a scan rate of 0.1mV/s and then anodically and cathodically polarised from +200mV to –1000mV.

3 Results and Discussions

3.1 Powder and Composite Characterisation

3.1.1 Particle Size Distribution

From the particle size distribution curve, the particle sizes of the as-received powders at d(50) for the Al alloy and SiC were found to be 11.993µm and 48.012µm respectively. After milling, the particle sizes then decreased to 4.439µm for Al alloy and 0.12µm for SiC. Figure 1 shows that the particle size distribution at d(50) for the composite with 30wt% SiC reinforcement was 0.489µm before sintering. The SiC milled for 16 hours and Al-30wt% SiC composite exhibited bimodal distributions.

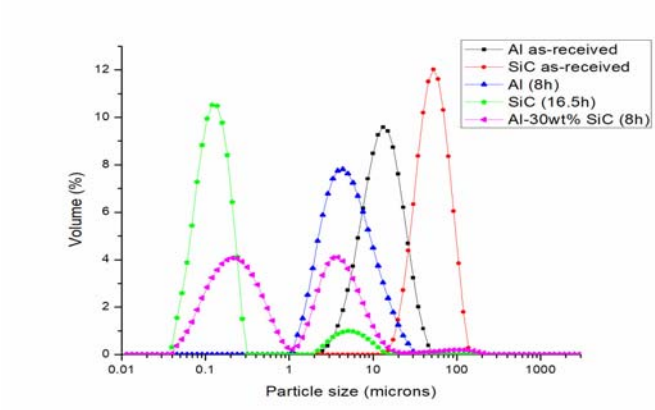

Figure 1: Particle size distribution curves of as-received and milled powders at d(50).

3.1.2 XRD Analysis

XRD identified no new phases, especially detrimental carbides such as Al_4C_3 and Al_4SiC_4. This can be attributed to solid-state sintering of the composites. Figure 2 shows the peaks intensities of SiC increased with increased SiC proportions in the composite, whereas the Al matrix peak intensities decreased less.

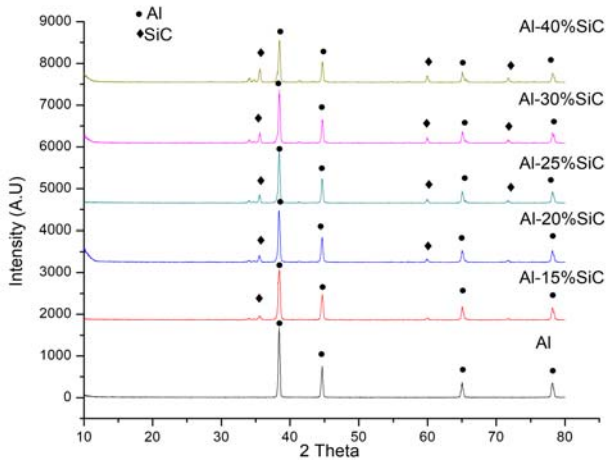

Figure 1: XRD patterns of milled Al-SiC composites

3.1.3 Microstructural Characterisation of Al-SiC Composites

Figure 3 shows optical micrographs of the Al composites reinforced with SiC of 15wt%, 20wt%, 25wt% and 40wt%. SiC were fairly distributed in the matrix. In areas where SiC was less, pools of Al alloy were noticed. This is probably due to the wide range of proportions of Al alloy in the samples.

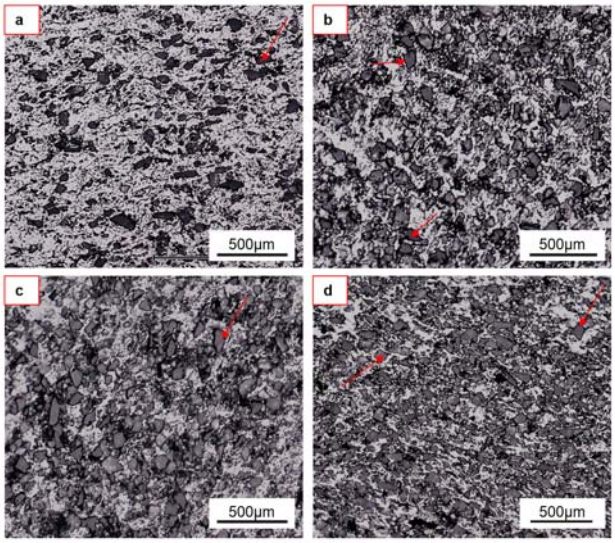

Figure 3: Optical micrographs of composites after sintering at 600°C: (a) Al-15wt%SiC, (b) Al-20wt%SiC, (c) Al-25wt%SiC, and (d) Al-40wt%SiC, where SiC has the darker contrast.

Figure 4(a) of the milled Al-20wt% SiC composite shows that SiC particles were often stuck on the Al alloy powders.

SPS is a pressure-aided solid-state sintering technique, andFigure 4(b) shows the sintering process during consolidation of the milled powder composites. An instantaneous decrease in temperature was observed when pressure was applied during the process, and a constant pressure was maintained during the 10mins dwell time at 600°C.

3.1.4 Density and Hardness Measurements

The actual densities of the composites increased with increased SiC content (Figure 5(a)). The relative densities were all above 97%, hence exhibiting the effectiveness of the SPS method. Furthermore, the increased proportions of SiC added to the ductile Al matrix, improved the hardness of the composite as expected, as shown in Figure 5(b).

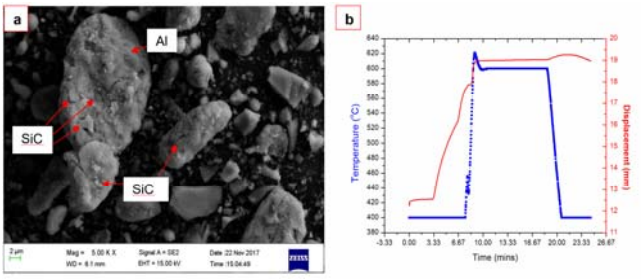

Figure 4: (a) SEM secondary electron image of Al-20wt% SiC powder milled for 8h, (b) sintering and displacement curves of an Al-SiC composite.

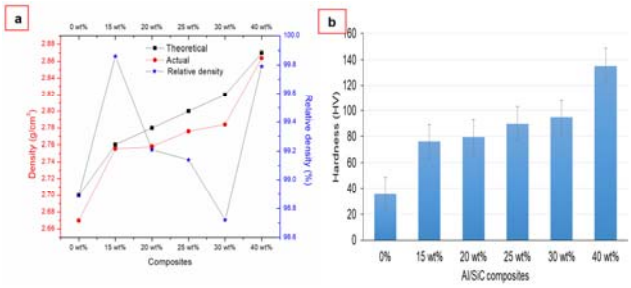

Figure 5: Properties of different composition SPS Al-SiC composites: (a) densities, and (b) average Vicker's hardness

3.2 Electrochemical Measurements

3.2.1 Corrosion Potential - Time Trends

Composites were immersed for 3200s at a scan rate of 0.05V/s, and their open circuit potentials (OCP) are presented in Table 1. The composites reinforced with 15 and 40wt% SiC exhibited shifts of potential in the more negative direction before stabilising at potentials of about -800mV and -700mV respectively. For 30wt% SiC containing composite, the potential approached the positive potential region. The trends observed for 20 and 25wt% SiC reinforced composites and the reference monolithic Al alloy were fluctuations of the applied potentials with time. This shows a tendency of localised corrosion, like pitting, to take place.[20]

Table 1 Open circuit potential (OCP), corrosion potential (vs Ag/AgCl) and corrosion current density of Al-SiC SPS composites immersed in 3.5wt% NaCl.

Composite	Open circuit potential, OCP (mV)	Corrosion potential, E_{corr} ($mV_{Ag/AgCl}$)	Corrosion current, I_{corr} (A/cm^2)
Al-0%SiC	-739	-897	2.379×10^{-5}
Al-15%SiC	-621	-645	9.447×10^{-7}
Al-20%SiC	-668	-738	9.225×10^{-5}
Al-25%SiC	-687	-701	1.487×10^{-3}
Al-30%SiC	-717	-726	7.304×10^{-4}
Al-40%SiC	-627	-729	2.061×10^{-3}

3.2.2 Tafel Polarisation Plots

The corrosion potentials obtained from the linear sweep voltammetry (LSV) test listed in Table 1 show the reference unreinforced Al alloy had an E_{corr} more negative than the composites. However, the corrosion resistance of the composites reinforced with 15 and 20wt% SiC improved with respect to its corrosion current density (I_{corr}) compared to the unreinforced Al alloy. The corrosion resistance of the other composites slightly decreased. Al-15wt% SiC exhibited the highest polarization resistance.

A grey layer formed on all the composites after exposure, with some tiny white spots, likely to be pits. With the Al alloy matrix being reactive, it formed a protective oxide layer, and it is speculated that the Cl^- ions in the 3.5wt% NaCl were adsorbed and occupied flaws in the protective film. These anions then formed soluble compounds which penetrated the film, leading to the pits. It is likely that sequentially, passive compounds Al_2O_3 and $Al(OH)_3$ were formed of lower energy and reacted with the Cl^- ions, forming aluminium complex ions and transitory complexes such as $AlCl^{++}$, $AlCl_4^-$, $Al(OH)Cl_2$ and $Al(OH)_2Cl$, culminating in the thinning of the oxide film.[9] The fundamental steps are summarized as[9]:

$$Al^{o} + 2Cl^{-} \longrightarrow AlCl_2\ (adsorbed) + 2e \quad (2)$$

$$AlCl_2\ (adsorbed) \longrightarrow AlCl_2^{+} + e \quad (3)$$

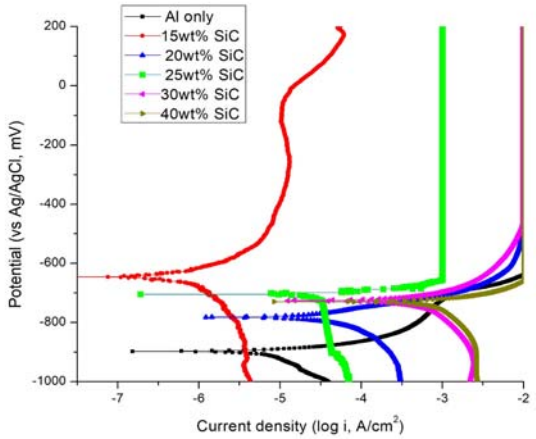

Figure 6: Tafel polarisation plots of SPS Al/SiC composites immersed in 3.5wt% NaCl solution.

4. Conclusion

Using the results obtained, the following conclusions were drawn:

- Al-SiC composites produced using SPS exhibited increased density with increased proportions of SiC.
- The hardness of the Al-SiC composites increased compared to the Al alloy, due to the SiC ceramic reinforcement to the ductile Al matrix.

Acknowledgements

Special thanks go to Dr Patrick Rokebrand of the University of the Witwatersrand (Wits) for all his assistance during experimentation.

References

1. D.B. Miracle, "Metal Matrix Composite – From Science to Technological Significance", Composite Science and Technology 65 (2005): pp. 2526–2540.

2. C. Sun, M. Song, Z. Wang, Y. He, "Effect of Particle Size on the Microstructures and Mechanical Properties of SiC-Reinforced Pure Aluminum Composites", Journal of Materials Engineering and Performance 20 (2011): pp. 1606–1612.

3. S. Min, "Effects of Volume Fraction of SiC Particles on Mechanical Properties of SiC / Al Composites", Transactions of Nonferrous Metals Society of China 19 (2009): pp. 1400–1404.

4. S. Bathula, R.C. Anandani, A. Dhar, A.K. Srivastava, "Microstructural Features and Mechanical Properties of Al5083 / SiCp Metal Matrix Nanocomposites Produced by High Energy Ball Milling and Spark Plasma Sintering", Materials Science and Engineering A 545 (2012): pp. 97–102.

5. Z. Zhang, F. Wang, J. Luo, S. Lee, L. Wang, "Microstructures and Mechanical Properties of Spark Plasma Sintered Al–SiC Composites Containing High Volume Fraction of SiC", Materials Science and Engineering A 527 (2010): pp. 7235–7240.

6. T.S. Mahmoud, E.Y. El-kady, A. Al-Shihri, "Corrosion Behaviour of Al/SiC and Al/Al2O3 Nanocomposites", Corrosion Engineering, Science and Technology 47 (2012): pp. 45–54.

7. P.C.R. Nunes, L.V Ramanathan, "Corrosion Behavior of Alumina-Aluminum and Silicon Carbide-Aluminum Metal-Matrix Composites", Corrosion 51 (1995): pp. 610–617.

8. Y. Shimizu, T. Nishimura, I. Matsushima, "Corrosion Resistance of Al-Based Metal Matrix Composites", Materials Science and Engineering A 198 (1995): pp. 113–118.

9. R.T. Foley, "Localized Corrosion of Aluminum Alloys — A Review", Corrosion 42 (1986): pp. 277–288.

10. A.J. Trowsdale, B. Noble, S.J. Harris, I.S.R. Gibbins, G.E. Thompson, G.C. Woods, "The Influence of Silicon Carbide Reinforcement on the Pitting Behaviour of Aluminium", Corrosion Science 38 (1996): pp. 177–191.

11. M. Metzger, S.G. Fishman, "Corrosion of Aluminum-Matrix Composites. Status report", Industrial and Engineering Chemistry Produst Research and Development 22 (1983): pp. 296–302.

12. M.M. Buarzaiga, S.J. Thorpe, "Corrosion Behavior of As-cast, Silicon Carbide Particulate-Aluminum Alloy Metal-Matrix Composites", Corrosion 50 (1994): pp. 176–185.

13. E. Maahn, S. Roepstorff, "Corrosion Resistance of Aluminium-Silicon Carbide Composite Materials", in 12th Riso Symposium of Metal Matrix Composites, eds. N. Hansen, D.J. Jensen, T. Leffers, H. Lilholt, T. Lorentzen, A.S. Pedersen, O.B. Pedersen, and B. Ralph (Roskilde, Denmark: Riso National Laboratory, 1990), p. 497.

14. I.B Singh, D.P. Mandal, M. Singh, S. Das, "Influence of SiC Particles Addition on the Corrosion Behavior of 2014 Al-Cu Alloy in 3.5% NaCl solution", Corrosion Science 51 (2009): pp. 234–241.

15. H. Sun, E.Y. Koo, H.G. Wheat, "Corrosion Behavior of SiCp/6061 Al Metal Matrix Composites", Corrosion 47 (1991): pp. 741–753.

16. M.S.N. Bhat, M. Surappa, H.. Sudhaker Nayak, "Corrosion Behaviour of Silicon Carbide Particle Reinforced 6061 / AI alloy composites", Journal of Materials Science 26 (1991): pp. 4991–4996.

17. S. Coleman, V.D. Scott, B. McEnaney, "Corrosion Behaviour of Aluminium-Based Metal Matrix Composites", Journal of Materials Science 29 (1994): pp. 2826–2834.

18. D. Landolt, S. Mischler, M. Stemp, "Electrochemical Methods in Tribocorrosion : A Critical Appraisal", Electrochimica Acta 46 (2001): pp. 3913–3929.

19. W.R. Matizamhuka, "Spark Plasma Sintering(SPS) – An Advanced Sintering Technique for Structural Nanocomposite Materials", The Journal of the Southern African Institute of Mining and Metallurgy 116 (2016): pp. 1171–1180.

20. N. Diomidis, P. Celis, J, P. Ponthiaux, F. Wenger, "A Methodology for the Assessment of the Tribocorrosion of Passivating Metallic Materials", Lubrication Science 21 (2009): pp. 53–67.

African Corrosion Journal
Official publication of the Corrosion Institute of Southern Africa
www.africorr.org.za

The electrochemistry and the prediction of stress corrosion cracking

Josias van der Merwe
University of the Witwatersrand and DST-NRF Centre of Excellence in Strong Materials
1 Jan Smuts Ave
Johannesburg, Gauteng, 2001
South Africa

ARTICLE INFO

Keywords:
Stress-corrosion cracking
Passivity
Stress Corrosion

ABSTRACT

Stress-corrosion cracking is very dependent upon the susceptible alloy and environmental interactions to either sustain cracking, or mitigate or inhibit it. Therefore, to understand this interaction, it is important to characterise the electrochemistry, and in particular the passivation characteristics of the alloy. Crack propagation occurs when passivation is disrupted by the strain of the underlying metal because of the application of an external force or residual stress. When the passive film on the metal is not very stable, this disruption is more likely and crack propagation becomes very dependent upon passivation characteristics, such as the passivation rate and the extent of passivation. Therefore, by understanding the passivation characteristics, it is possible to determine the mechanism of crack propagation and identify the parameters that influence the propagation rate. In addition, it becomes possible to predict the susceptibility to cracking, as well as possibly monitor the electrochemical noise in order to detect cracking. This was investigated in various stress-corrosion sensitive systems where the passivation characteristics were compared to stress-corrosion susceptibility while parameters, such as temperature, were altered to influence crack propagation rates. The correlation between passivity and crack sensitivity can be used to predict the extent of cracking once a relationship has been established for a particular system. However, it remains difficult to make an exact prediction because of various parameters that influence cracking, especially during the crack initiation stage. Although detecting and monitoring crack activity in certain systems was possible, it should be evaluated further.

1. Introduction

Stress corrosion has been difficult to predict and in many instances the onset and propagation of cracks are not easily predictable[1]. This is dependent upon a number of factors that have to be described, but cracking occurs generally in two distinct stages, crack initiation and propagation[2]. The initiation stage could occur over an extended period of time and might require very specific conditions to enable the crack to form. When these conditions are not met, cracking will not occur, and many times under plant conditions this is exactly the reason why the system might not lead to cracking[3]. This of course could lead to finding ways to mitigate the cracking process, but first of all it is important to understand the parameters that would enhance the crack initiation process. Stress corrosion occurs when there exists a fine balance between the transition from passivation to localised corrosion[4]. With the application of stress, the passive film is disrupted when a slip step emerges on the surface where the passive film has formed. This disruption can be enhanced by the slow passivation of the freshly

exposed metal, or can be reformed to ensure continuous passivation. Therefore, when the balance between passivation and local corrosion is at a certain level, the formation of a crack becomes possible. If corrosion is enhanced, this could lead to pitting corrosion, or in the most severe case, uniform corrosion. However, when passivation is very effective complete passivation will occur no cracking will result. Generally, the passive-active transition zones have been identified as electrochemical potential regions where cracking will occur with greater ease. It was the aim of this study to investigate this passivation character through the electrochemical nature, and then to compare this with the crack sensitivity as determined with slow strain-rate test results. Therefore, would it be possible to predict the extent of cracking from the electrochemical characteristics of the cracking process? Two systems were investigated to determine various sensitivities and the extent of cracking of very different material-environment combinations, and protective mechanisms. One of these systems was investigated previously to determine the extent of passivation required to inhibit cracking completely[5]. This is helpful, since at the point of sufficient passivation, the cracking might even be enhanced. The embrittlement of a high strength steel exposed to low pH aqueous conditions was analysed over a wide temperature range. These results were compared to a system found in low carbon pressure vessel steel exposed to a carbon monoxide-carbon dioxide environment, where the effect of corrosion was altered by the addition of an inhibitor[5].

2. Experimental Procedure

A high strength steel was evaluated and the chemical analyses of the steel used were obtained by optical emission spectroscopy and the results are shown in Table 1.

3.0 Results and Discussions

The slow strain-rate test results of the samples exposed to the low pH environment are shown in Table 2.

The nature of the cracks found were intergranular in places, as shown in the tempered martensitic microstructure in Figure 1.

The nature of the cracks on the surface of the steel sample seen with a stereo microscope are shown in Figure 2.

The polarisation characteristics of the steel at 45°C was investigated, and the results are shown in Figure 3. Here the absence of a passive region was evident.

Table 1 Bulk composition of the high strength steel

	C	Mn	S	P	Si	Cr	Mo	Ni	Cu	Al	V	Nb	Co	Fe
Weight %	0.14	1.25	≤0.005	0.01	0.23	0.41	0.05	0.08	0.02	0.074	0.015	0.006	0.019	Balance

Table 2 Slow strain-rate test results at various temperatures

Temperature	d_0	l_0	d_f	A_0	A_f	% Red. in Area
35°C	5.0	25.2	4.0	19.8	12.6	36.7
45°C	5.1	24.7	4.5	20.4	15.8	22.5
55°C	5.0	24.0	4.6	19.6	17.0	13.7
65°C	5.0	24.0	4.6	19.6	16.8	14.6

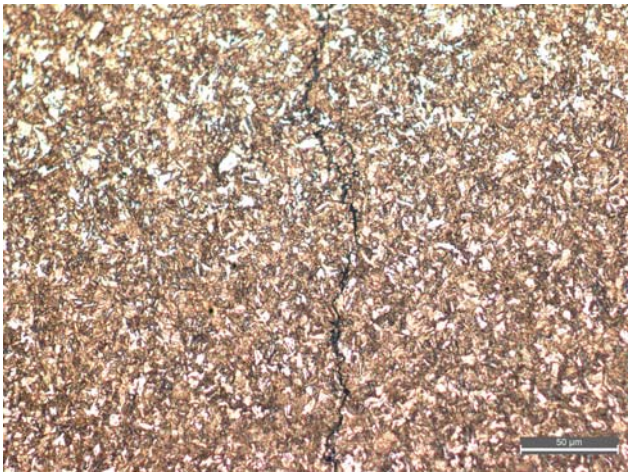

Figure 1: Tempered martensitic structure of the steel with a typical crack running through the centre.

Figure 2: Secondary surface cracks on the sample tested at 65°C.

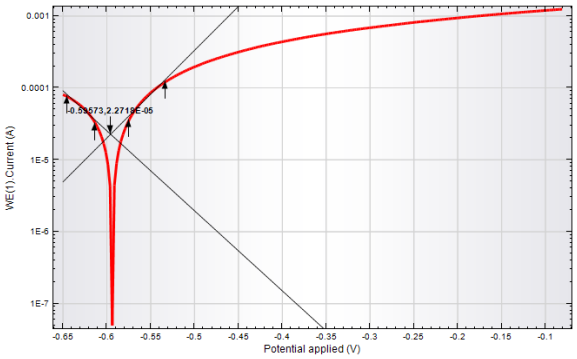

Figure 3: Polarisation characteristics of the steel in the environment at 45°C.

3.1 Passivation and sensitivity to cracking of steel in CO-CO_2-H_2O

In the carbon monoxide-carbon dioxide-water system, the effect of passivation was much more significant as shown in Figure 4. Here, a pressure vessel A516 grade 70 steel was used for the tests as described previously[6]. The nature of passivation was significantly affected by temperature and was especially pronounced at the high carbon monoxide concentration. Carbon monoxide falls in the category of an adsorption inhibitor (Heusler[7]) and therefore inhibits the corrosion process of the steel by strong chemisorbtion8[4]. This was confirmed for iron, on which it reacts slowly to form carbonyl, which is not stable in acid solutions[7], making carbon monoxide not a very effective inhibitor, but one that could be disrupted by slip steps.

Cotton and Wilkinson[9] indicated that carbon monoxide possessed an electronic structure similar to cyanide, in that it is a reproducing complexing ligand which bonds with the metal atom via the carbon atom. Here, the weak electron donor properties of the molecule and the vacant orbitals of the metal are involved with the corrosion reaction, as suggested by Trabanelli[10].

The carbon monoxide molecule has a pair of electrons strongly directed away from the carbon-oxygen bond[7], which facilitate adsorption on a metal with unfilled electron levels. Carbon monoxide is not adsorbed on zinc, and does not inhibit zinc dissolution as found by King and Rau[12]. They found that carbon monoxide was not completely effective as an inhibitor, since during weight loss experiments, there was some weight loss, even after short exposure times, which is usually not true for pure adsorption inhibitors. The reason for this ineffectiveness might be the slow adsorption of carbon monoxide to protect certain regions, as found by Heusler[7]. Carbon monoxide adsorbs reversibly on iron in sulphuric acid. The adsorption caused a slight shift in potential, but the overall effect was seen on the anodic polarisation curve, with a considerable diminution of the corrosion rate. This slow adsorption of the carbon monoxide strongly influenced the stress-corrosion sensitivity of the steel.

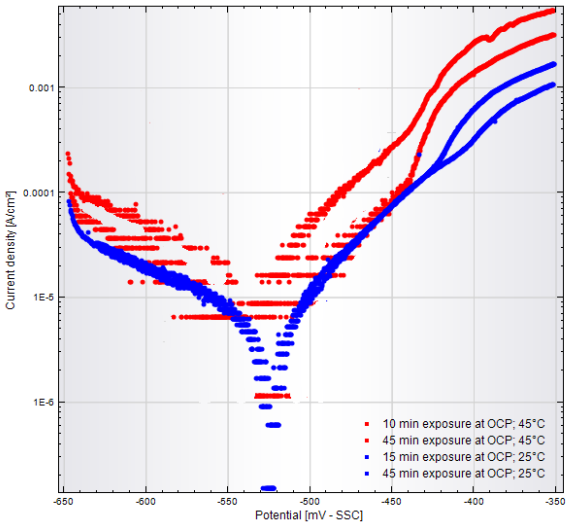

Figure 4: Polarisation characteristics of A516 pressure vessel steel exposed to 50% CO – 50% CO_2 at 800 kPa, at a scan rate of 0.1 mV/s after being held at open circuit potential (OCP)

for various times from 1 minute to 5 hours. Blue curves were performed at 25°C and the red curves at 45°C[13].

From slow strain-rate results, it was shown that the steel exposed to 50% CO-50% CO_2 (800 kPa) at 45°C was considerably more susceptible to cracking than for the same mixture at 25°C. From the curves shown in Figure 4, it is clear that the extent of passivation increased by several orders of magnitude with the increase in temperature. Not only was the passive region more pronounced at 45°C, but also the passivation was influenced by the time exposed to the environment. The curves shown in Figure 4 were determined in the same environment, although not only at two temperatures, but also different exposure times of 10 and 15 minutes as well as 45 minutes. While the exposure time was not exactly the same time for the shorter exposure, the extent and influence on inhibition was clear. At the short exposure time and 25°C the passive region was not significantly different from where the curve would have been in the active state. However, after 45 minutes, the passive region had extended slightly and even in the active region, beyond -390 mV, the curve showed an overall drop in current density values. This time dependent passivation of the steel surface was different at the higher temperature where the stress corrosion susceptibility was also more significant. For 45°C, the current density difference was more apparent between the active region, beyond -430 mV, and the passive region, which was where the stress corrosion susceptibility also increased. In addition, after 45 minutes the difference between the passive region and the active projected curve (not shown) was also more after 15 minutes. It is important to note that the severity of the environment-metal interaction was increased with a faster passivation rate. Therefore, a fine balance exists between the passivation rate and the crack propagation rate.

3.2 Inhibited steel in CO-CO_2-H_2O environment

As shown by Van der Merwe and Du Toit[6] for steel in the carbon monoxide-carbon dioxide system, the passivation required for complete inhibition with no crack initiation or propagation was significant. When passivation was improved by the addition of a corrosion inhibitor, the susceptibility to cracking even increased when the inhibitor concentration was too low. The polarization characteristics of the steel showed that when the passive current density decreased from 100 μA/cm^2 to approximately 10 μA/cm^2, the inhibition was sufficient to remove sensitivity to cracking. However, the extent of the passive region in the inhibited state was over a long range and not the short passive potential range of around 80 mV found on the 25% CO-75% CO_2 system at 45°C. The shape of the passive region actually changed completely, and the active region was removed for the potential region being evaluated.

4. Conclusion

From these three systems described, it was clear that the dependence of cracking on the passivation of the steel varied widely. The high strength steel did not show any signs of passivation, but its sensitivity to cracking increased with temperature. The cracking mechanism in this case related to hydrogen embrittlement, considering the high strength of the steel and the presence of the hydrogen reaction at low pH levels. The carbon monoxide-carbon dioxide system showed a definite relationship between crack propagation and passivation. When passivation was significant and occurring at a high enough rate, crack propagation was sustained. However, to completely inhibit cracking, it was necessary to add an inhibitor, which extended the passive range over a much larger potential region. Therefore, to predict cracking from the passivation would be difficult and this should be considered only by understanding the passivation rate and loading rates, and especially the mechanism causing embrittlement. However, once cracking has been established, the measure of passivation might give a qualitative indication of cracking susceptibility.

References

1. M. Kowaka and S. Nagata, "Transgranular stress-corrosion cracking of mild steels and low-alloy steels in H_2-CO-CO_2 systems," Corrosion 24, 12 (1968): p. 427 – 429.

2. R.N. Parkins, "Significance of pits, crevices, and cracks in environment-sensitive crack growth," Material Science Technology 1, (1985): p. 480.

3. R.H. Jones and R.E. Ricker, "Mechanism of stress-corrosion cracking," 1st ed. (Materials Park, Ohio: ASM International, 1992): p. 8.

4. A. Brown, J.T. Harrison and R. Wilkins, Corrosion Science, 10 (1970), p. 547.5. J. W. van der Merwe, "Environmental and Material Influences on the Stress-Corrosion Cracking of Steel in H_2O-CO-CO_2 Solutions," International Journal of Corrosion, vol. 2012, Article ID 414156, (2012): 13 pages.

6. J.W. van der Merwe and M. du Toit, "Mitigation of stress corrosion cracking of carbon steel exposed to CO-CO_2-H_2O environments through inhibitor addition," Anti-Corrosion Methods and Materials 60, 6 (2013): p. 295 – 300.

7. K.E. Heusler, G.H. Cartledge, "The influence of iodide ions and carbon monoxide on the anodic dissolution of active iron," Journal of the Electrochemical Society 108, 8 (1961): p. 732-740.

8. C. De Waard, D.E. Milliams, Corrosion 31, 5 (1975): p.177.

9. F.A. Cotton, G. Wilikinson, Advanced inorganic chemistry, 611, Interscience, (1968).

10. G. Trabanelli, F. Zucchi, G.I. Zucchini, "Influence du mono-oxyde de carbone sur les processus de dissolution des mètaux," Corrosion - Traitement protection finition 16, 7 (1968): p. 335-345.

11. H.B. Urbach, L.G. Adams, R.E. Smith, Journal of the Electrochemical Society 55, (1974): p391.

12. C.V. King, E. Rau, Journal of the Electrochemical Society, 103, (1956): p. 331.

13. J.W. van der Merwe, The stress-corrosion cracking of carbon steel in CO-CO_2-H_2O, PhD thesis, University of Pretoria (Pretoria, 2013), p. 118.

African Corrosion Journal
Official publication of the Corrosion Institute of Southern Africa
www.africorr.org.za

Benchmarking international cathodic protection and alternating current mitigation standards to determine suitable protection criteria

Craig Botha
Reignite (Pty) Ltd
Durban, South Africa

ARTICLE INFO

Keywords:
Benchmarking
Cathodic
Protection
Alternating; Current
SP0169
EN50162
EN13509
ISO15589-1
TM0497
RP0104
SP0177
EN15280
SP21424
Current
Density
Corrosion

ABSTRACT

From time to time international standards are withdrawn, amended, updated or new standards are introduced that change the current thinking on existing subject matter. This paper demonstrates the complex process of reviewing a number of prominent Cathodic Protection and Alternating Current Mitigation standards and then attempting to benchmark suitable protection criteria. Today common Right of Way issues exist due to the convergence of pipelines, high voltage powerlines, telecommunications and other services that produce an environment conducive to rapid corrosion on previously secure pipeline assets.

In this paper we review aspects of ISO15589-1 Part 1, NACE SP0169, EN50162, EN13509, NACE TM0497, NACE RP0104 and the work of NACE International Task Groups 210 and 211. In addition to these classical works relating to Cathodic Protection, this paper gives attention to aspects of the contemporary Alternating Current standards and reports namely NACE SP0177, BS EN 15280, NACE SP21424-2018 and NACE International Technical Report 35110.

As these documents are unpacked and assessed it soon becomes evident that the exclusive use of Cathodic Protection in a highly congested Right of Way does not guarantee that corrosion will be curtailed on well coated, buried steel pipelines.

Some comments and recommendations are made to guide the thinking of engineers, pipeline owners and operators towards applying suitable designs and more importantly monitoring the most critical variables in predicting the probability of corrosion in complex Alternating Current and Direct Current environments.

1. Introduction

The past 20 years in the field of Cathodic Protection (CP) have ushered in the distinct shift from the assessment of conventional Direct Current (DC) corrosion mechanisms to the more complex world of electrochemistry influenced by Alternating Current corrosion mechanisms. In fact traditional assessment of CP protection levels

without taking cognizance of the AC interference on a structure can have catastrophic consequences for pipeline operators. The most common misnomer over the past 20 years has been the idea that a pipeline under suitable levels of CP cannot corrode in a High Voltage Powerline Right of Way.

Extensive amounts of research and in-field investigations have revealed that AC corrosion is now a significant element of pipeline integrity assessment and the emphasis over two decades has been to update standards, the introduction of AC mitigation systems and the real life assessment of the probability or likelihood of AC corrosion in areas where CP criteria appear to be acceptable. This paper will firstly assess recent thinking on the measurement of DC structure-to-electrolyte potentials, secondly provide some insight into developments around AC structure-to-electrolyte potential measurements and thirdly provide guidelines being used to assess the likelihood of corrosion based on ratio of AC current density to DC current density at simulated coating defect sites on a typical buried pipeline.

2. Direct Current Structure to Electrolyte Potential Measurements

A number of standards, reports and documents are considered here and relevant portions are highlighted from each to develop a picture of current thinking.

2.1. ISO15589-1 Petroleum and Natural Gas Industries - Cathodic Protection Of Pipeline Transportation Systems. Part 1 on-land pipelines[1]

Specific reference is made to paragraph 5.3 Criteria for CP and the sub-clauses contained therein as we have extracted some key points from this standard:

- The acceptable metal-to-electrolyte potential at which the corrosion rate is less than 0.01mm per year is the protection potential, Ep. This considered acceptable and within limits for the design life. The criterion for CP is therefore E ≤ Ep, where E is the polarized structure potential.
- Some metals can be subject to hydrogen embrittlement at very negative potentials, and coating damage can also increase at very negative potentials. For such metals, the potential shall not be more negative than a limiting critical potential El. In such cases, the criterion for CP is El ≤E ≤ Ep.
- The CP system shall be capable of polarizing all parts of the buried pipeline to potentials more negative than −850 mV referred to a saturated Copper Sulphate Reference Electrode (CSE), and to maintain such potentials throughout the design life of the pipeline. These potentials are those which exist at the metal-to-environment interface, i.e. the polarized potentials.
- To prevent damage to the coating, the limiting critical potential should not be more negative than −1200 mV referred to CSE, to avoid the detrimental effects of hydrogen production and/or a high pH at the metal surface. It must be noted that this criterion is unlikely to be achieved in South Africa due to the influence of Stray Current emanating from the extensive DC Traction Railway network. For high strength steels (specified minimum yield strength greater than 550 MPa), the limiting critical potential shall be determined with respect to the detrimental effects in the material due to hydrogen formation at the metal surface.
- For pipelines operating in anaerobic soils and where there are known, or suspected, significant quantities of sulfate-reducing bacteria (SRB) and/or other bacteria having detrimental effects on pipeline steels, potentials more negative than −950 mV referred to CSE should be used to control external corrosion.
- For pipelines operating in soils with very high resistivity, a protection potential more positive than −850 mV referred to CSE may be considered, e.g. as follows: −750 mV for 100 < ρ < 1000; −650 mV for ρ >1 000 where ρ is the soil resistivity, expressed in ohm metres.
- As an alternative to the protection potentials given above, a minimum of 100 mV of cathodic polarization between the pipeline surface and a reference electrode contacting the electrolyte may be used.

- The application of the 100 mV polarization criterion shall be avoided at higher operating temperatures, in SRB-containing soils, or with interference currents, equalizing currents and telluric currents. The conditions should be characterized prior to using this criterion. Furthermore, the criteria shall not be used in case of pipelines connected to or consisting of mixed metal components. Under certain conditions, pipelines suffer from high-pH Stress Corrosion Cracking (SCC) in the potential range −650 mV to −750 mV, and this shall be considered when using protective potentials more positive than −850 mV.
- For pipelines operating at temperatures above 40 °C, the above values may not provide adequate protection potential. In these cases, alternative criteria shall be verified and applied.

2.2. NACE SP0169-2013 Control of External Corrosion on Underground or Submerged Metallic Piping Systems[2]

Specific reference is made to paragraph 6.2.2 Steel and Cast Iron Piping and the sub-clauses contained therein as we have extracted some key points from this standard:

- A negative (cathodic) potential of at least 850 mV with the CP applied. Voltage drops other than those across the structure-to-electrolyte boundary, relative to a saturated copper/copper sulfate reference electrode, must be considered for valid interpretation of this voltage measurement.

  NOTE: Consideration is understood to mean the application of sound engineering practice in determining the significance of voltage drops by methods such as:

  i. Measuring or calculating the voltage drop(s);
  ii. Reviewing the historical performance of the CP system;
  iii. Evaluating the physical and electrical characteristics of the pipe and its environment; and
  iv. Determining whether or not there is physical evidence of corrosion.

- A negative polarized potential of at least 850 mV relative to a saturated copper/copper sulfate reference electrode.
- A minimum of 100 mV of cathodic polarization between the structure surface and a stable reference electrode contacting the electrolyte. The formation or decay of polarization can be measured to satisfy this criterion.
- In some situations, such as the presence of sulfides, bacteria, elevated temperatures, acid environments, and dissimilar metals, the criteria set above may not be sufficient.
- When a pipeline is encased in concrete or buried in dry or aerated high-resistivity soil, values less negative than the criteria listed above may be sufficient.
- Polarized potentials less negative than -850 mV for CP of pipelines is not advised when operating pressures and conditions are conducive to stress corrosion.
- The use of excessive polarized potentials on externally coated pipelines should be avoided to minimize cathodic disbondment of the coating. This caution is not easily applied in South Africa due to the effects of Stray Current emanating from the use of widespread DC Traction Railway networks.
- Excessive generation of hydrogen related to very negative pipe-to-soil potentials should be avoided on all metals, particularly higher-strength steel.

2.3. EN50162 Protection Against Corrosion by Stray Current from Direct Current Systems[3]

The most notable aspect of the standard is the introduction of anodic and cathodic interference concepts in terms of DC sources of interference. This warrants further attention, but would be best suited to another technical paper dedicated to DC interference.

2.4. EN13509 Cathodic Protection Measurement Techniques[4]

Specific reference is made to paragraph 4.4 Potential Measurement Techniques and the sub-clauses contained therein as we have extracted some key points from this standard:

- Measuring technique including IR drop (on potential measurement). These are potential measurements conducted while the protective current is on are referred to as "on potential measurements". On potentials, E_{on}, contain various unknown IR drops, which can change with time and position of the reference electrode. The readings do not reflect the potential at the metallic electrolytic phase boundary.

- Measuring techniques to determine IR free potentials ($E_{IR\ free}$). A number of measurements are taken under the category of IR free potential measurements namely:

  i. *Off potential measurements (instantaneous off potential technique)* may be used to eliminate IR drops caused by protective current) where equalizing currents, cells currents due to foreign anodes or foreign cathodes and stray currents are not present. The values obtained are referred to as off potentials, E_{off}. This is typically achieved by carrying out a Close Interval Potential Survey (CIPS).
  ii. *Special off potential measurements* may be applied in areas, where DC Stray Current activity is present, during intervals in which the DC Traction system is not in operation.
  iii. *Intensive measurement technique* may be used to cover IR drops caused by equalizing currents, cell currents, and, fluctuating or not fluctuating currents from remote foreign sources. Simultaneous measurements are taken of pipe-to-soil potentials and associated horizontally opposed potential gradients. The technique identifies coating defects and enables calculation of IR free potentials at the defects. This technique is suitable in the linear portion of the potential gradient caused by the remote current source. Intensive measurements are made to determine the IR free potential (EIR free) at coating holidays detected by various methods such as DCVG (Direct Current Voltage Gradient) Survey, CIPS (Close Interval Potential Survey) or PCM (Pipe Current Mapper) Survey.
  iv. *Potential measurements for pipelines with external potential test probes or coupons* may be used to cover IR drops caused by protective current, equalizing currents, cell currents, and fluctuating or not fluctuating currents from remote or nearby foreign sources. This technique is particularly useful if the structure is within the non-linear part of the potential gradient (where potential gradients are not constant with distance) caused by a (nearby) foreign current source.

2.5. TM0497 Measurement Techniques Related to Criteria for Cathodic Protection on Underground or Submerged Metallic Piping Systems[5]

Specific reference is made to paragraphs 5.10 and 5.11. In addition to these paragraphs Sections 8, 9 and 10 have specific test methods that are referred to below. We have extracted some key points from clauses 5.10 and 5.11:

- 5.10 Essentially all voltage drops shall be considered, other than those across the metal/electrolyte interface, for valid interpretation of pipe-to-electrolyte voltage measurements made to satisfy a criterion. Measurement errors should be minimized to ensure that accurate pipe-to-soil potential measurements are recorded.
- 5.11 Interrupting all significant current sources and then making the measurement permits elimination of all significant IR drop components. This measurement is referred to as an “instant- off” potential.
- Section 8: Test Method 1—Negative 850 mV Pipe-to-Electrolyte Potential of Steel and Cast Iron Piping with Cathodic Protection Applied.
- Section 9: Test Method 2—Negative 850 mV Polarized Pipe-to-Electrolyte Potential of Steel and Cast Iron Piping.
- Section 10: Test Method 3—100 mV Cathodic Polarization of Steel, Cast Iron, Aluminum, and Copper Piping.

2.6. NACE SP0104-2014 The Use of Coupons for Cathodic Protection Monitoring Applications[6]

Steel coupons are used extensively in the field to enable the measurement of surrogate coating

defect behavior. Figure 1 shows a typical steel coupon arrangement.

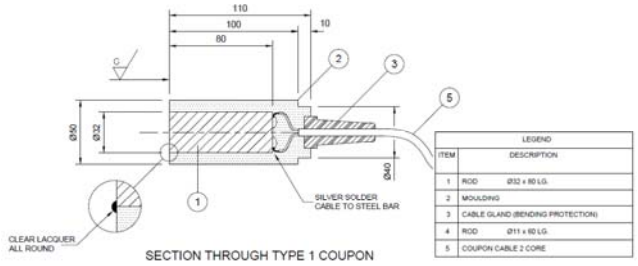

Figure 1: Typical Steel Coupon Construction

In NACE SP0104-2014 specific reference is made to paragraphs 1.3, 3.3, 3.7 and the sub-clauses contained therein as we have extracted some key points from this standard:

- Structure-to electrolyte potentials may be obtained without interrupting multiple CP sources.
- Where direct-connected galvanic anodes are used coupons can assist with measuring instant- off potentials.
- Depolarization testing may be performed in most cases without de-energizing the CP system.
- Coupons permit accurate measurement of structure-to-electrolyte potentials on structures affected by stray currents.
- CP coupon polarized (off) potential is not identical to the conventional structure-to-electrolyte off potential measured from the surface of the ground. The structure-to electrolyte off potential is affected by many factors detailed in the standard.
- Coupons may be used when any of the following conditions occur:
  i. measuring or calculating the voltage drop(s);
  ii. multiple rectifiers must be interrupted synchronously;
  iii. foreign CP systems are present in the area and interruption thereof is problematic;
  iv. presence of stray current that causes significant IR-drop errors in the off-potential measurement;
  v. locally corrosive areas in an otherwise noncorrosive environment;
  vi. presence of spikes immediately following interruption that cause errors in the off-potential measurement;
  vii. multiple pipelines in the same right-of-way that produce interference with one another;
  viii. pipelines under the influence of alternating current; and
  ix. instances where no known CP problem exists, but uncertainty exists about existing data measurements.

2.7. NACE RP0104-2004 The Use of Coupons for Cathodic Protection Monitoring Applications. NACE International Task Group 210 - Coupon Technology - Technical Report on the Application and Interpretation of Data from External Coupons Used in the Evaluation of Cathodically Protected Metallic Structures[7]

Specific reference is made to a paragraph on page 15 CP Coupon Potential versus Structure Potential and the sub-clauses contained therein as we have extracted some key points from this report:

- The CP coupon potential is not exactly the same as the structure potential under investigation. The same holds true for the above ground potential measured during a close interval potential survey (CIPS) where the "measured potential" is assumed to be "the potential of the structure." Neither the CP coupon potential nor the CIPS potential is equivalent to the potential of the structure.
- Potential readings from the CIPS technique and CP coupons must be kept in perspective.
- Measurements above ground sample a potential field produced from a mixture of holidays. The CIPS measurements depend on coating defect size, distribution, coating quality, and the distance between the reference electrode and the structure.
- The CIPS technique can provide a trend over the length of a structure.
- The CP coupon potential is a point source of information, normally a picture of the potential in a localized environment. CP coupon measurements provide an indication of CP system effectiveness on a similarly sized

coating defect on a structure in the same localized environment.

2.8. NACE International Task Group 211 - on Cathodic Protection: Report on the Application of the 100 mV Polarization Criterion. One Hundred Millivolt (mV) Cathodic Polarization Criterion[8]

Specific reference is made to a paragraph on page 20 Use of CP Coupons to Measure Polarization and the sub-clauses contained therein as we have extracted some key points from this report:

Conditions generally arise when currents that affect polarization cannot be interrupted, such as in the following situations:

i. Dynamic stray currents (telluric, transit, induced AC, etc.) that substantially affect the structure;
ii. Circulating currents,
iii. Multiple influencing CP current sources that make simultaneous interruption impractical, and
iv. Multiple interconnected and cathodically protected pipelines in the same Right-of-Way.

- Coupons installed according to NACE Standard RP0104, the coupons are often used to evaluate polarization growth or depolarization under the conditions listed above.
- This report provides an indication of the increase in the use of the 100 mV cathodic polarization criterion from 26% to 76% in a 10 year period. However, survey respondents reported using the 100 mV cathodic polarization criterion on only 11% their systems, suggesting the trend toward more widespread use of the 100 mV cathodic polarization criterion.
- Increased usage of the 100 mV criterion is probably influenced by the increased application of the –850 mVCSE polarized potential criterion. Although this may be associated with incorrectly interpreted sub-criterion of the –850 mVCSE current applied criterion.

3 Alternating Current Structure To Electrolyte Potential Measurements

A few pertinent references relating to AC corrosion are extracted from prominent specifications to highlight how the assessment of purely DC potentials and current densities can be perilous.

3.1 NACE SP0169-2013 Control of External Corrosion on Underground or Submerged Metallic Piping Systems[2]

- Clause 6.2.1.4.5. introduces AC current densities (I_{AC}) at which AC corrosion is likely to occur at significant levels and that additional CP polarization is not necessarily good:

i. I_{AC} > 30A.m^{-2} AC corrosion may be significant.
ii. I_{AC} > 100A.m^{-2} AC corrosion may be expected even if CP criteria is satisfied.
iii. Under some soil conditions increasing CP polarization can increase AC corrosion significantly as shown in Figure 2.

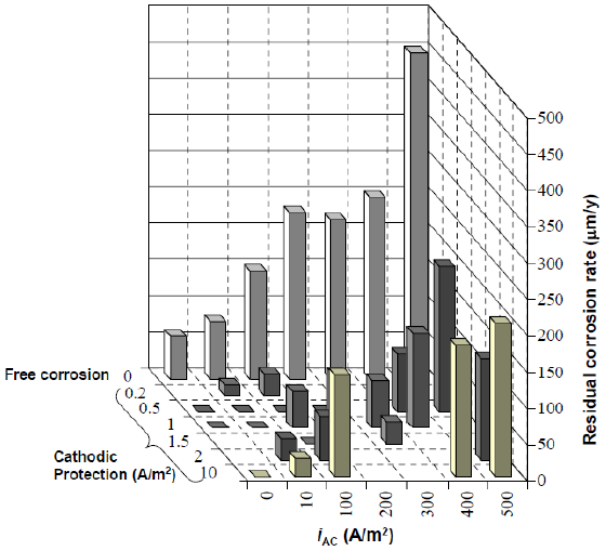

Figure 2 Residual Corrosion Rate of Carbon Steel Specimens as a Function of AC and CP Current Density. Laboratory Tests Performed in Simulated Soil Conditions[9]

3.2 NACE International Technical Report 35110, AC Corrosion State-of-the-Art: Corrosion Rate, Mechanism, And Mitigation Requirements[10]

On page 7, of this report, last paragraph, "Considering that the primary factor in

determining the possibility for the presence of AC corrosion is the AC density, monitoring the current density rather than the AC voltage is used to assess the AC-related hazards to a buried pipeline." This statement speaks directly to the opinion and current thinking of multiple other technical papers that support the use of coupons for the measurement of both AC and DC current densities.

Once the magnitude of the AC and DC current densities is known the likelihood of AC corrosion can be assessed in a more reliable manner than would be the case when inferring the likelihood of AC corrosion from AC structure-to-soil potentials and surrounding soil resistivity measurements.

3.3 BS EN 15280-2013: Evaluation of AC Corrosion Likelihood of Buried Pipelines Applicable to Cathodically Protected Pipelines[11]

This standard considers the assessment of the likelihood of AC corrosion on the basis of measuring a number of key variables namely:

- AC voltage on the structure
- ON Potential
- IR-free potential
- AC current density
- DC current density
- AC/DC current density ratio
- Soil resistivity
- Corrosion rate.

Figures 3 and 4 below summarize AC and DC current limits as well as AC and DC voltage limits at which AC corrosion is likely to occur.

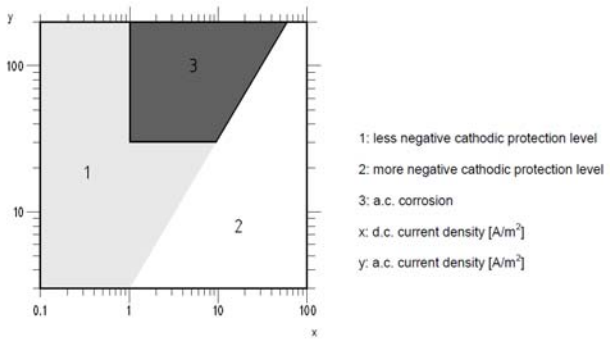

Figure 3 : Likelihood of AC Corrosion. AC Current Density vs DC Current Density[11]

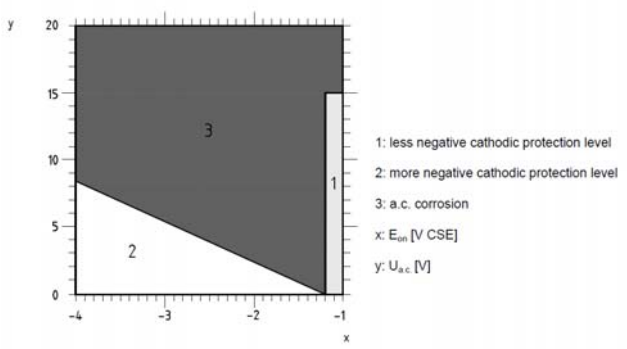

Figure 4 Likelihood of AC Corrosion. AC Potential Uac vs DC On Potential E_{on}[11]

3.4 NACE SP21424-2018: Alternating Current Corrosion on Cathodically Protected Pipelines: Risk Assessment, Mitigation and Monitoring[12]

This standard sets out key contributing factors in the evaluation and mitigation of AC Corrosion with specific emphasis on the following:

- Analysis (Risk Assessment)
- Mitigation Strategy
- Monitoring Strategy
- Monitoring
- Safe Operating Conditions

The ISO and EN standards have tended to highlight the influence of AC current density, DC current density, soil resistivity, cathodic polarization and the scenarios that may contribute to AC Corrosion. This standard is more specific in the following key areas soil resistivity, AC current density and DC current density.

- On page 7, clause 5.4.4 states, " The following soil resistivity parameters can be applied as a guideline to corrosion risk:
  - Below 25Ω.m: very high risk,
  - Between 25 and 100Ω.m: high risk,
  - Between 100 and 300Ω.m: medium risk,
  - Above 300Ω.m: low risk."
- On page 7, clause 5.4.6 Coupon or Corrosion Rate Probe Measurements introduces the relationship between coupon and corrosion rate probe measurements and the specific criteria established on page 8 under Clause 6.2, "Current Density: Unless effective AC corrosion control has been otherwise document, the AC current density should not exceed a time- weighted average of:
  - 30A.m^{-2} if DC current density exceeds 1 A.m^{-2}

- 100A.m^{-2} if DC current density is less than 1A.m^{-2}

4. Conclusion

From the benchmarking exercise it is evident that there are key measurement requirements under both DC and AC conditions that merit particular mention. A few are highlighted below:

- Neither the polarized structure to electrolyte potential of -850mV to a saturated copper / copper sulphate reference electrode nor the 100mV polarization criteria guarantee protection of buried metallic structures where significant AC current densities exist at coating defect sites.[2]
- DC current density and potential measurements alone are not sufficient to ensure that a buried steel structure will be protected.[11]
- The use of steel coupons in the assessment of CP criteria is well establish and considered essentially to address key errors such as IR drop, no defect frame of reference, not baseline to assess DC current density.[6]
- Intensive testing techniques are available to support field work in such a manner that IR drop and DC interference conditions can be assessed in a meaningful manner.[4]
- Recent work done in assessing AC corrosion has revealed that at AC current densities of more than 30A.m^{-2} AC corrosion may occur, while at AC current densities exceeding 100A.m^{-2} AC corrosion is almost certain even though DC CP criteria are met.[2]
- The ratio of AC current density to DC current density should ideally be less than 3 to minimize the likelihood of AC corrosion.[11]
- Coupons may be used for AC corrosion and AC current density assessment.[11]
- AC voltage and soil resistivity measurements are no longer supported as general indicators of the likelihood of AC corrosion, but are rather part of an overall assessment where the ratio of AC current density to DC current density is favoured as a more conclusive guideline.[2,10,11]

Acknowledgements

Craig Botha thanks Transnet Capital Projects, eThekwini Water Services, Transnet Pipelines and Mr Martin Lebenya of Paradigm Projects for the opportunity to present the findings of review reports and ongoing field work on projects that are not identified by name for a variety of reasons.

References

1. ISO15589-1 Petroleum and Natural Gas Industries - Cathodic Protection of Pipeline Transportation Systems. Part 1 On-Land Pipelines.
2. NACE SP0169-2013 Control of External Corrosion on Underground or Submerged Metallic Piping Systems.
3. EN50162 Protection Against Corrosion By Stray Current From Direct Current Systems.
4. EN13509 Cathodic Protection Measurement Techniques.
5. TM0497 Measurement Techniques Related to Criteria for Cathodic Protection on Underground or Submerged Metallic Piping Systems.
6. NACE SP0104-2014 The Use of Coupons for Cathodic Protection Monitoring Applications.
7. NACE RP0104-2004 The Use of Coupons for Cathodic Protection Monitoring Applications. NACE International Task Group 210 - Coupon Technology - Technical Report on the Application and Interpretation of Data from External Coupons Used in the Evaluation of Cathodically Protected Metallic Structures.
8. NACE INTERNATIONAL TASK GROUP 211 - On Cathodic Protection: Report on the Application of the 100 mV Polarization Criterion. One Hundred Millivolt (mV) Cathodic Polarization Criterion.
9. M. Ormellese, L. Lazzari, A. Brenna, A. Trombetta, "Proposal for CP Criterion In The Presence of AC - Interference," Corrosion201, Paper No. 32 (Houston, TX: NACE, 2010).
10. NACE International Technical Report 35110, AC Corrosion State-Of-The-Art: Corrosion Rate, Mechanism, and Mitigation Requirements.
11. BS EN 15280-2013: Evaluation of AC Corrosion Likelihood of Buried Pipelines Applicable to Cathodically Protected Pipelines.
12. NACE SP21424-2018: Alternating Current Corrosion on Cathodically Protected Pipelines: Risk Assessment, Mitigation and Monitoring.

African Corrosion Journal
Official publication of the Corrosion Institute of Southern Africa
www.africorr.org.za

Pipeline integrity management in oil and gas production facilities through corrosion mitigation and inspection strategy: an experience of Arabian Gulf Oil Company (AGOCO), Libya

Iftikhar Ahmad
Technical Affairs Department
Arabian Gulf Oil Company (AGOCO), Libya

ARTICLE INFO

Keywords:
Pipeline integrity management
Corrosion mitigation and inspection

ABSTRACT

Poor integrity of pipelines is one of the major causes of leaks and accidents in oil and gas production and transportation facilities. The primary objective of pipeline integrity management (PIM) is to maintain pipelines in a fit-for-service condition, while extending their remaining life in the most reliable, safe and cost effective manner. A successful pipeline integrity management program incorporates aspects of design, material selection, operations, maintenance, corrosion mitigation, monitoring and inspection, risk evaluation and communication concepts to maximize the return from pipelines. The objective of a corrosion management plan is to define all necessary activities to assure the integrity of the pipelines by control of corrosion. This will ensure consistent availability and safe operation of the pipelines in an oilfield throughout the specified design life. The objective should be achieved in the most cost- effective manner, by designing for mitigation of corrosion, for inspection and monitoring and for maintenance in a timely manner.

Under these circumstances, it has become crucial to manage operational risk through the use of effective technology and best practices for inspection and maintenance planning. External corrosion on pipelines is controlled with a combination of coatings and cathodic protection while internal corrosion is controlled with a combination of chemical inhibitors, periodic cleaning and process control. The monitoring and inspection techniques provide a way to measure the effectiveness of corrosion control systems and provide an early warning when changing conditions may be causing a corrosion problem.

Arabian Gulf Oil Company (AGOCO) is one of the subsidiary companies of National Oil Corporation of Libya. It owns several oilfields and two refineries in Libya and it has an oil export terminal. This paper presents the experience of management of oil and gas pipelines through corrosion mitigation, corrosion monitoring and inspection strategy in AGOCO oilfields, based on standard practices of corrosion mitigation and inspection.

1. Introduction

Pipeline integrity management is a process for assessing and mitigating pipeline risks in order to reduce both the likelihood and consequences of incidents. For liquid pipelines, the U.S. Department of Transportation addresses pipeline integrity management[1] in the U.S. Code of Federal Regulations (CFR) Title 49 Part 195. The oilfields of Arabian Gulf Oil Company (AGOCO) have large network of pipelines. AGOCO is one of the

subsidiary companies of National Oil Corporation (NOC) of Libya. It owns Sarir, Messla, Majid, Nafoora, Beda and Hamada oilfields. Another two new oilfields namely Sultan and Karim oilfields, are in development in Libya. The length and diameter of pipelines in AGOCO oilfields are shown in Tables 1 to 3.

Table 1: AGOCO shipping pipelines and their lengths.

Name	Diameter (inch)	Length (km)	Year of Construction	Name of Fluid
Sarir - Tobruk	34	513.6	1966	Crude Oil
Sarir - GMMRA	16	90	1990	Gas
Sarir - Messla	30	41.2	1982	Crude oil
Messla - Amal	42	205.5	1982	Crude oil
Messla - Sarir	20	42.5	1982	Gas
Majed - Nafoora	14	106	1968	Crude oil
Nafoora - Amal	24	52	2013	Crude oil
Nafoora oilfield – 103A oilfield	24/16	36.6/31.9	1967/68	Crude oil
Hamada - Zawia	18	386	1968	Crude oil
Beda - Tibesti	12/14	27.2	1970	Crude oil

Table 2: AGOCO trunklines and their lengths

Name	Diameter (inch)	Length (km)	Year of Construction	Name of Fluid
Sarir Oilfield				
GC4 - GC1	24	22	1966	Fluid (oil, gas, and water)
GC6 - GC1	12	12	1967	Fluid (oil, gas, and water)
GC5 - GC1	12	11,5	1967	Fluid (oil, gas, and water)
GC3 - GC1	24	18.5	1966	Fluid (oil, gas, and water)
GC2 - GC1	18	12	1966	Fluid (oil, gas, and water)
Messla Oilfield				
GC7 - GC 9	18	7.06	1982	Crude Oil
GC7 - GC9	10	7.06	1982	Gas
GC8 - GC9	20	11.86	1982	Crude oil
GC8 - GC9	12	11.86	1982	Gas
GC10 - GC9	12	5.43	1982	Crude oil
GC10 - GC9	8	5.43	1982	Gas
Nafoora Oilfield				
GOSP3 – CPS	20	9.8	1970	Crude oil
GOSP3 - CPS	16	9.8	1970	Low Pressure Gas
GOSP4 - CPS	20	12	1970	Crude oil
GOSP4 - CPS	8	12	1970	High Pressure Gas
GOSP4 – GOSP6 (Balance Line)	8	6	2001	Crude oil
GOSP4 - GOSP6	10	6	1980	Low Pressure Gas
GOSP4 - GOSP8	8	12	1988	High Pressure Gas
GOSP5 - CPS	10	5.3	1991	Crude oil
GOSP5 to Tie-in (GOSP4 - CPS)	16	4	1996	Crude oil
GOSP7 – CPS	12	12	1978	Crude oil
GOSP8 – GOSP4	16	12	1988	Low Pressure Gas
GOSP8 - CPS	16	17.6	1978	Crude oil
GOSP9 - CPS	12	N/A	1991	Fluid (oil, gas, and water)
Area L – GOSP K	12	11.4	2012	Fluid (oil, gas, and water)
Area O – GOSP K	12	26.2	2012	Fluid (oil, gas, and water)
GOSP K – GOSP3	12	12.1	2012	Fluid (oil, gas, and water)
Majed Oilfield				

Name	Diameter (inch)	Length (km)	Year of Construction	Name of Fluid
Majed2 – Majed1	12	26	1992	Crude oil
Beda Oilfield				
Warid – CPS	12	21.8	-	Crude oil
Kotla – CPS	10	14.4	1986	Crude oil
Bulawn – Dor	8	8.2	-	Crude oil
Dor – Kotla	6	22.8	1986	Crude oil
GS1 – CPS	6	8.34	1995	Crude oil
GS3 – CPS	6	3.7	1995	Crude oil
Mansour – Dor	8	3.85	-	Crude oil
Hamada Oilfield				
CR-0004 – NC-8	6	6.5	-	Fluid (oil, gas, and water)
CR-0008 – NC-8	6	9.5	-	Fluid (oil, gas, and water)
CR-0009 – NC-8	6	31.25	-	Fluid (oil, gas, and water)
CR-0001 – NC-8	8	29	-	Fluid (oil, gas, and water)
CR-0004 – NC-8	8	3.5	-	Fluid (oil, gas, and water)
CR-0007 – NC-8	8	25	-	Fluid (oil, gas, and water)
CR-0009 – NC-8	8	9.5	-	Fluid (oil, gas, and water)
CR-0004 – NC-8	10	3.6	-	Fluid (oil, gas, and water)
CR-0009 – NC-8	10	22.2	-	Fluid (oil, gas, and water)
CR-0006 –NC-8	12	21	-	Fluid (oil, gas, and water)

Table 3: Flow lines and their lengths at different AGOCO oilfields

Name of Oilfield	No. of Flow Lines	Size of Flow Lines (inch)	Length of Flow Lines (m)
Sarir	353	4, 6 & 8	977,152
Nafoora Unit Area	133	4,6, 8 & 10	420,576
Nafoora Non-Unit Area	135	4 & 6	263,338
Hamada	106	3 & 4	293,421
Messla	126	4 & 6	378,924
Majid	25	4 & 6	138,608
Beda (including Dor, Kotla and Umm Farud)	79	3.5 & 4	138,682

Degradation of pipelines is the result of the persistent attack by the external environment on pipeline materials (pipes, welds, coatings, etc.) and the characteristics of fluids flowing in the pipeline. The most prevalent threat to a pipeline is corrosion. Corrosion is a time-dependent phenomenon. There are two types of corrosion: (i) external corrosion, and (ii) internal corrosion. External corrosion is a major factor contributing to the deterioration of buried pipeline; it weakens the pipe wall, which increases the risk of failure. External corrosion is a function of the interaction between the pipeline and the soil that surrounds it. The aggressiveness of soil towards steel is affected[2] by soil properties such as resistivity, pH, and presence of sulfate reducing bacteria. Dissimilar soils can affect a buried pipeline, as they will encounter soils that have varying compositions. Variations in weather and tides can change the corrosion conditions of submerged pipelines.

Various chemical species present within pipelines can significantly affect internal corrosion[3] in the system. Factors that have significant effects on the corrosion rate in pipelines are:

- Water content
- Acid gases (CO_2 and H_2S)
- Oxygen
- Chlorides
- Solids
- Paraffin, waxes, and asphaltenes
- Flow velocity
- Temperature
- Pressure
- pH
- Pipeline material
- Sulfate - reducing bacteria

A small change in one of these parameters can change the corrosion rate considerably, due to changes in the properties of the thin layer of corrosion products that accumulates on the steel surface. Pipeline materials are susceptible to various forms of physical degradation due to interactions between the material and the environment. The physical degradation may be in the form of uniform metal loss, isolated/localized (pitting) metal loss, environmentally assisted cracking, or flow assisted damage as shown in Figure 1.

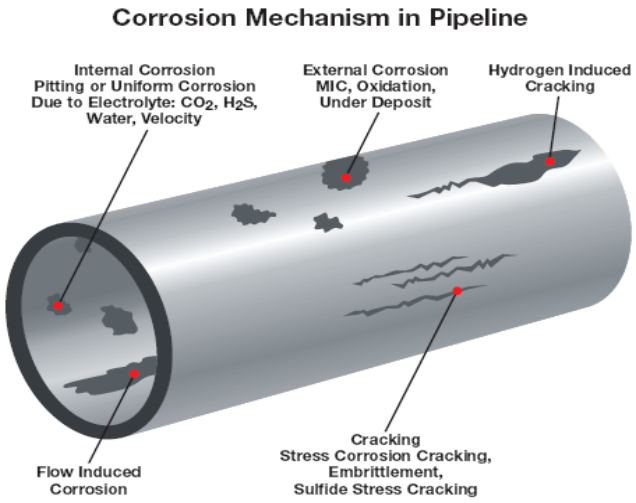

Figure 1: Corrosion mechanisms in pipelines

The other factors which also contribute to the pipeline integrity are discussed below:

Soil Conditions - Soil structure and conditions contribute to the creation of corrosive environment of the buried pipelines. Factors such as soil type, drainage, temperature, and resistivity of soil all contribute to the environment surrounding the pipe.

Temperature – The temperature of the soil, as well as the temperature of the pipe, may create favorable conditions for attack on pipeline materials. Liquid and gas pipelines have slightly different operating temperature characteristics, but both are still susceptible.

Stresses (Residual and Others) – Stresses in the pipe may lead to premature degradation of pipeline strength. The stresses acting on the pipe include:

a) residual stress from the manufacturing process,

b) external stress such as those incurred due to bending, welding, mechanical gouges, and corrosion, and

c) secondary stresses due to soil settlement or movement.

Pipe Pressure – Corrosion, in particular cracking, is related to the pressures exerted on the pipe. As the pressures within the pipe are increased, the growth rates for cracks also increase. The circumferential stress (hoop stress) generated by the pipeline operating pressure is usually the highest stress component that exists.

Cyclic Loading Effects – Conditions where the pipe is under cyclic loads may result in increased crack growth rates. The pipeline pressure continually fluctuates due to loading and unloading of product and is influenced by pump activity. This applies to both gas and liquid lines, but has greater influence in liquid systems.

2. Mitigation of Corrosion on Pipelines for Agoco Oilfields

2.1. External Corrosion

High performance pipeline coatings/wrappings and cathodic protection (CP) are used to combat external corrosion[4,5] on pipelines in AGOCO oilfields. CP is achieved in practice by one of two primary types of CP systems, including sacrificial anode (galvanic anode) CP and impressed-current CP. Sacrificial anode CP utilizes an anode material that is electronegative to the pipe material. When connected to the pipe, the pipe becomes the cathode in the circuit and corrosion is mitigated. Typical sacrificial anode materials for underground pipelines are zinc and magnesium.

Impressed-current CP utilizes an external power supply (rectifier) to control the voltage between the pipe and the anode (cast iron, graphite, platinum clad, mixed metal oxide, etc.) in such a manner that the pipe becomes the cathode in the circuit and corrosion is mitigated.

CP is used in conjunction with a coating/wrapping for AGOCO pipelines. There are always flaws in the coating due to application inconsistencies, construction damage, or the combination of natural aging and soil stresses. The effect of these factors on corrosion mitigation is discussed below:

Disbonded Coatings - The most significant corrosion problem on coated and cathodically protected pipeline is that of disbonded pipeline coatings that shield cathodic protection when disbondments occur, and water penetrates between the coating/wrapping and the pipe. All coatings can and will disbond for various reasons. Poor application procedures, soil stress, temperature and a variety of other reasons can cause coatings to disbond.

Holidays and Coating Damage – A holiday is defined as a discontinuity in coating, when a part of the surface remains uncoated. Holidays also include other type of defects, such as lack of bonding, pinholes, cracks in coating, and insufficient or excessive film thickness. If holidays or damage occur during the coating application, during construction or during the burial of the pipeline, these areas can become spots where corrosion can occur, but are not usually a corrosion problem if CP is adequate. One problem that exists with the proposed changes in the criteria as quoted in NACE SP0169 standard is that many companies will be using more and more stringent criteria trying to meet a polarized – 850 mV or more negative potential at all sites on the pipeline system. This will cause more cathodic disbondment that may lead to more shielding of the CP current from the pipe by coatings that shield.

Holidays should be located and repaired as the pipe is being installed in the ditch, but a proper repair with the proper repair material must be performed. Many times the repair material will lose adhesion and may shield the CP allowing corrosion to occur.

AC and DC Stray Current Interference - Corrosion caused from AC or DC stray current interference can be very rapid, causing significant damage to metal surfaces from which the current discharges into the electrolyte. This type of corrosion will cause failure long before the design life of the system is reached. If not detected and corrected quickly, the interference will result in leaks and potential explosions and environmental disaster. This corrosion is usually easily detected through various surveying methods such as close interval/or direct current voltage gradient surveys.

Shielding from Other materials - Shielding can be caused from materials that are around a pipeline other than coatings. During the design phase of the pipeline it is critical not to use materials that will cause CP shielding. Some of these materials are solid, non-conductive rock shield, various plastic construction materials not removed from the pipe or ditch, high resistant sand or rock backfill, metal structures in close proximity, reinforced concrete structures and other metal structures that may pick up the CP current intended for the pipeline.

Inadequate Cathodic Protection - This is the least likely cause of corrosion on cathodically protected and coated pipelines. With the use of ILI (In-Line Inspection) tools and ECDA (External Corrosion Direct Assessment), the true causes of external corrosion on these systems are now being proven. If companies, government agencies, and contractors will spend more time training their employees on the proper evaluation techniques for determining the cause of external corrosion, the industry will find that inadequate CP is not the likely cause of corrosion.

2.2. Internal Corrosion

Internal corrosion is also an electrochemical process; however, CP is not a viable option for mitigation internal corrosion in a pipeline. One of the first defense systems against corrosion for transmission pipelines is to ensure that the product being transported is free of moisture. Dry, aerated natural gas and moisture-free oil are not corrosive. To maintain crude oil free of water is not possible. It always has traces of water. For corrosion to occur, there must be moisture, CO_2, oxygen, H_2S, or some other reduction reactants, such as one produced by sulfate-reducing bacteria (H_2S). Operators typically control moisture, oxygen, H_2S and CO_2 contents of the transported oil or gas, but these constituents can enter the pipeline through compressor or pump stations, metering stations, storage facilities, or other means.

Chemical inhibitor programs are used in AGOCO oilfields to mitigate internal corrosion. Corrosion inhibitors for mitigate corrosion and biocides to prevent biological activity are used. In pipelines which flow fluid having a scale-forming tendency, scale inhibitors are used to prevent scaling. Periodical cleaning by pigging is also performed in AGOCO pipelines to prevent internal corrosion.

Chemical inhibitor programs are used in AGOCO oilfields to mitigate internal corrosion. Corrosion inhibitors for mitigate corrosion and biocides to prevent biological activity are used. In pipelines which flow fluid having a scale-forming tendency, scale inhibitors are used to prevent scaling. Periodical cleaning by pigging is also performed in AGOCO pipelines to prevent internal corrosion.

3. Corrosion Monitoring And Inspection

The monitoring and inspection techniques[7] provide a way to measure the effectiveness of the corrosion control systems and provide an early warning when changing conditions may be causing a corrosion problem. The rate of corrosion dictates how long a pipeline can be safely operated. Corrosion monitoring techniques can help in several ways:

- by providing an early warning that damaging process conditions exist which may result in a corrosion-induced failure.
- by studying the correlation of changes in process parameters and their effect on system corrosivity.
- by diagnosing a particular corrosion problem, identifying its cause and the rate controlling parameters, such as pressure, temperature, pH, flow rate, etc.
- by evaluating the effectiveness of a corrosion control/prevention technique, such as chemical inhibition and the determination of optimal applications.
- by providing management information relating to the maintenance requirements and ongoing condition of a pipeline.

3.1. Internal Corrosion Assessment

The severity of internal corrosion of a pipeline can be determined[8] using corrosion monitoring techniques and the extent of corrosion damage is determined using inspections and assessments. Modelling is a tool for estimating corrosion rate and identifying monitoring locations. Corrosion rate models can be used to determine the effect of gas or liquid constituents on the corrosion rate of a pipeline.

3.1.1. Corrosion Rate Modelling

Corrosion rate models can be (i) *Mechanistic* – use the electrochemical reaction to determine a corrosion rate; (ii) *Empirical* – use experimental results to determine a correlation for the corrosion rate; or (iii) *Combination of both* – models based on electrochemical reactions but are then adjusted using experimental data.

NACE SP0208 Standard, "Internal Corrosion Direct Assessment Methodology for Liquid Petroleum Pipelines"[9] provides descriptions of various corrosion rate models. Modeling requires knowledge of operating conditions and gas and/or liquid quality data. Typical operating conditions include pressure, temperature, and flow rate (at a minimum). Gas quality data includes moisture content, CO_2, H_2S, and O_2 content. Liquid quality includes basic sediment and water (BS&W) content in fluid in the pipeline, and water analysis data, including pH.

3.1.2. Corrosion Monitoring Techniques

The corrosion monitoring techniques can be classified as:

a) Direct methods – involve the measurement or quantification of metal loss, from which corrosion rates can be estimated

b) Indirect methods – monitor parameters that can influence, or are influenced by the corrosion severity of the pipeline contents

c) Intrusive methods – require penetration into the pipe or vessel to gain direct access to the interior of the equipment

d) Non-intrusive methods – can monitor internal pipe wall loss from the outside of the pipe or vessel wall

Sampling methods are considered intrusive methods because access to the interior environment is required to obtain a sample. Table 4 lists and describes the characteristics of monitoring techniques commonly used.

Table 4: Types of Monitoring Techniques

	Direct	Indirect
Intrusive	• Corrosion coupons • Spool pieces • Electric Resistance (ER) probes • Linear Polarization Resistance (LPR) probes • Electrochemical Noise (ECN)	• Hydrogen probes • Water chemistry • Solid analysis • Gas analysis
Non-Intrusive	• Ultrasonic testing (UT) • Electrical Field Mapping (EFM)	• Hydrogen patch probes • Acoustic monitoring

Corrosion monitoring devices only provide information about the specific location where they are installed. Therefore, carefully selecting representative locations to monitor internal corrosion is essential in order to collect data that are meaningful. Proper selection requires knowledge of the internal environment and the system design.

Additional methods of analysis include scanning electron microscopy (SEM) and energy dispersive spectroscopy (EDS). SEM analysis can determine corrosion severity and morphology on a microscopic scale using 500X to 1000X (or higher) magnifications. EDS determines the qualitative chemical composition of scales or deposits associated with corrosion features on the coupon. Table 5[10] provides general interpretations that can be made from coupon monitoring results.

Table 5: Categorization of Carbon Steel Corrosion Rates from NACE SP 0775[10]

Severity of Corrosion	Average Corrosion Rate		Maximum Pitting Rate	
	(mm/y)	(mpy)	(mm/y)	(mpy)
Low	< 0.025	< 0.1	< 0.13	< 0.50
Moderate	0.025–0.12	1.0–4.9	0.13–0.20	5.0–7.9
High	0.13–0.25	5.0–10	0.21–0.38	8.0–15
Severe	> 0.25	>10	> 0.38	>15

3.2. Inspection Methods

Inspection methods are used to detect and evaluate damaged areas. Inspection techniques provide information on the extent of corrosion damage. However, they do not provide information on the time period over which the corrosion occurred. When inspection methods are performed at regular intervals, they can be used as a monitoring technique. The commonly used inspection techniques are: (i) Visual inspection, (ii) Magnetic flux leakage (MFL), (iii) Ultrasonic testing (UT), (iv) Guided wave ultrasonic testing (GWUT), (v) Eddy current (ED), and Radiographic testing (RT).

3.2.1 In-Line Inspection (ILI)

In-line inspection tools, also referred to as smart or intelligent pigs, are devices that are propelled in the pipeline and are used to detect and characterize metal loss caused by corrosion. There are two primary types of ILI tools: magnetic flux leakage (MFL) tools and ultrasonic tools (UT). The more advanced ILI tools (high-resolution tools) are capable of discriminating between internal and external corrosion.

A magnetic flux leakage inspection pig uses magnetism to detect changes in the thickness of the pipe wall. The pipe wall is magnetized using a strong magnet. Any metal-loss in the pipe wall will cause the induced magnetic field to change. This change can be sensed using a detector and hence metal-loss defects can be identified. Post-processing of the collected data can be used to size and in some cases characterize (i.e. manufacturing, corrosion, etc.) the features identified in the pipeline. Magnetic flux leakage pigs can be run in both liquid or gas pipelines (i.e. they do not require a liquid couplant) and are capable of measuring metal-losses, even in thin-walled pipes. The inspection provides a relative (i.e. percentage wall thickness) measurement of defect depth.

Another type of commonly used intelligent pig is the ultrasonic inspection pig. An ultrasonic inspection pig uses ultrasound to detect changes in the thickness of the pipe wall. A transducer transmits signals perpendicular to the pipe wall surface and receives signals back from both the internal and the external surface of the pipe wall. The time taken to receive the signals can then be used to determine the wall thickness of the pipeline. Ultrasonic pigs must be run in a liquid, since they require a couplant. They give an absolute measurement of defect depth and have the advantage that they can measure metal-losses in much thicker pipes than is possible with magnetic flux leakage technology.

Although the principle is very simple, UT tools also have some drawbacks. The first, and arguably the most important, is that they cannot normally be used to inspect gas pipelines as the sound will only travel through a homogeneous liquid. The

word "homogeneous'' is almost as important as the word "liquid" in this context, as such things as gas bubbles and wax flocculation can affect the results.

MFL tools measure the change in magnetic flux lines produced by the defect and produce a signal that can be correlated to the length and depth of a defect. In recent years, the magnetic, data storage, and signal interpretation have improved, resulting in improved mapping of the flaw and a decrease in the number of unnecessary excavations. The high-resolution MFL tool is typically capable of readily detecting corrosion pits with a diameter greater than three times the wall thickness. Once detected, these tools can typically size the depth of the corrosion within +10 percent of the wall thickness with an 80 percent level of confidence. The MFL tools can used to inspect either liquid products pipelines or natural gas pipelines.

3.3. External Corrosion Direct Assessment

External corrosion direct assessment (ECDA) is a structured process that is intended to improve safety by assessing and reducing the impact of external corrosion on pipeline integrity[11]. It is explained in NACE standard practice SP 0502 – 2010. It is based on following four steps:

The Pre-Assessment Step – The "Pre-Assessment" step involves the collection and evaluation of historical data and pipeline characteristics. Based on this information, the feasibility of an ECDA application is determined and once affirmed, the pipeline is divided into regions with similar exposure and areas where the same indirect inspection tools may be used.

The Indirect Inspection – The "Indirect Inspection" step uses a combination of two or more above ground survey techniques such as close interval potential survey (CIPS), alternating current voltage gradient (ACVG), direct current voltage gradient (DCVG), AC attenuation for the identification of areas with corrosion activities or coating faults. The data is evaluated via systematic analysis and high-risk areas are identified for excavation.

The Direct Examination – The "Direct Examination" step covers the selection of sites to be excavated and the physical identification of defects requiring repair or replacement.

The Post Assessment – The "Post Assessment" step evaluates the previous three steps of the ECDA process and establishes a future assessment schedule.

Acknowledgement

I acknowledge the help and support of management and staff of Technical Affairs Department of AGOCO.

References

1. DOT Regulation 49 CFR Part 195," Pipeline Safety: Pipeline Integrity Management in High Consequence Areas (Hazardous Liquid Operators with less than 500 miles of pipeline)". Research and Special Programs Administration (RSPA), U.S. Department of Transportation (DOT) Federal Register, Vol. 67, No. 11 (2002), pp. 2136 – 2144.

2. M. A. Alodan, and F. Abdulaleem, "Pipeline Corrosion in Soil", King Saud University, Deanship of Scientific Research, Research Centre – College of Engineering, Final Research Report No. 425/17 (2007).

3. E.W. Klechka, "Pipeline Integrity Management and Corrosion Control", Materials Performance, pp. 24 – 27 (2002).

4. R. Norsworthy, "Coatings used in Conjunction with Cathodic Protection – Shielding Vs Non-shielding Pipeline Coatings", published by NACE International, Paper No. 4017 (2009).

5. NACE Standard Recommended Practice SP0169 – 2013, "Control of External Corrosion on Underground or Submerged Metallic Piping Systems", Published by NACE International in 2013.

6. A. Dugstad, L. Lunde, and S. Nesic, "Control of Internal Corrosion in Multi-Phase Oil and Gas Pipelines", Presented in Prevention of Pipeline Corrosion Conference, organized by Pipe Line Industry and Pipes & Pipelines International, held at Houston (Texas), USA on October 17 – 20 (1994).

7. J.S. Smart, and T. Pickthall, "Internal Corrosion Measurement Enhances Pipeline Integrity", Pipeline & Gas Journal, October 2004.

8. NACE Standard SP0102, "In-Line Inspection of Pipelines", Published by NACE in 2017.

9. NACE Standard SP0208, "Internal Corrosion Direct Assessment Methodology for Liquid Petroleum Pipelines", Published by NACE in 2008.

10. NACE Standard SP0775, "Preparation, Installation, Analysis, and Interpretation of Corrosion Coupons in Oilfield Operations", Published by NACE in 2013.

11. NACE Standard SP0502, "Pipeline External Corrosion Direct Assessment Methodology", Published by NACE in 2010.